

Design, Synthesis, and Biological Evaluation of Peptidomimetic Aldehydes as Broad-Spectrum Inhibitors against Enterovirus and SARS-CoV-2

Wenhao Dai,[○] Dirk Jochmans,[○] Hang Xie,[○] Hang Yang,[○] Jian Li, Haixia Su, Di Chang, Jiang Wang, Jingjing Peng, Lili Zhu, Yong Nian, Rolf Hilgenfeld, Hualiang Jiang, Kaixian Chen, Leike Zhang,* Yechun Xu,* Johan Neyts,* and Hong Liu*Cite This: <https://doi.org/10.1021/acs.jmedchem.0c02258>

Read Online

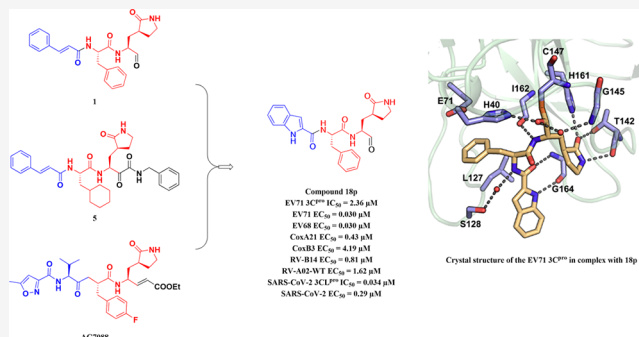
ACCESS |

Metrics & More

Article Recommendations

Supporting Information

ABSTRACT: A novel series of peptidomimetic aldehydes was designed and synthesized to target 3C protease (3C^{PRO}) of enterovirus 71 (EV71). Most of the compounds exhibited high antiviral activity, and among them, compound **18p** demonstrated potent enzyme inhibitory activity and broad-spectrum antiviral activity on a panel of enteroviruses and rhinoviruses. The crystal structure of EV71 3C^{PRO} in complex with **18p** determined at a resolution of 1.2 Å revealed that **18p** covalently linked to the catalytic Cys147 with an aldehyde group. In addition, these compounds also exhibited good inhibitory activity against the 3CL^{PRO} and the replication of severe acute respiratory syndrome coronavirus 2 (SARS-CoV-2), especially compound **18p** (IC₅₀ = 0.034 μM, EC₅₀ = 0.29 μM). According to our previous work, these compounds have no reasons for concern regarding acute toxicity. Compared with **AG7088**, compound **18p** also exhibited good pharmacokinetic properties and more potent anticoronavirus activity, making it an excellent lead for further development.



INTRODUCTION

Enterovirus 71 (EV71) belongs to the enterovirus genus of the picornaviridae family, and the genome of EV71 is composed of a single-stranded positive-sense RNA. To the best of our knowledge, EV71 is not only the primary pathogen of hand, foot, and mouth disease (HFMD) but also closely associated with neurological syndromes such as severe encephalitis and aseptic meningitis, and these diseases caused by the EV71 have become a worldwide health problem. Especially, young children are more susceptible to be infected by the enterovirus.¹ However, to date, there are no approved drugs to prevent or treat the associated diseases.² Considering the detriment of HFMD and the central neurological syndromes in children, the development of effective antiviral drugs is urgently needed.

The genome of enterovirus 71 encodes a polyprotein precursor, which is cleaved by the 3C protease (3C^{PRO}) and 2A protease (2A^{PRO}) into structural proteins and nonstructural proteins, of which the 3C^{PRO} is responsible for most of the cleavages. The 3C^{PRO} of enteroviruses and rhinoviruses (RV) is essential for viral replication, and it not only shared a high degree of homology at an amino acid level but also contained a Cys-His-Asp/Glu catalytic triad. In addition, the 3C^{PRO} is an exceptional cysteine protease with unique folding and catalytic mechanism, and a Gln is almost required in the P1 position of the substrates.

As far as we know, none of the known human proteases possessed a similar cleavage specificity, which makes 3C^{PRO} become a highly prospective target for developing broad-spectrum drugs.^{3,4} Recent efforts in drug discovery also furnished several inhibitors against the EV71 3C^{PRO} (Figure 1). Those peptidomimetic compounds with a warhead in P1' and a lactam ring in P1 could be briefly divided into reversible and irreversible inhibitors according to their binding modes. Compounds 1–6 are reversible inhibitors, among which compounds 1, 2, 4, and 5 are covalent reversible inhibitors, while 3 and 6 are noncovalent inhibitors. Those compounds exhibited good anti-EV71 activity with EC₅₀ values in the range of 0.009–3.7 μM, while the broad-spectrum antiviral activity and the drug-like properties were rarely evaluated.⁵ Rupintrivir (**AG7088**)^{5a} was reported to have the excellent antiviral activity against EV71 with an EC₅₀ value of 0.009 μM and has entered clinical trials as a protease inhibitor targeting rhinovirus 3C^{PRO},

Special Issue: COVID-19

Received: December 29, 2020

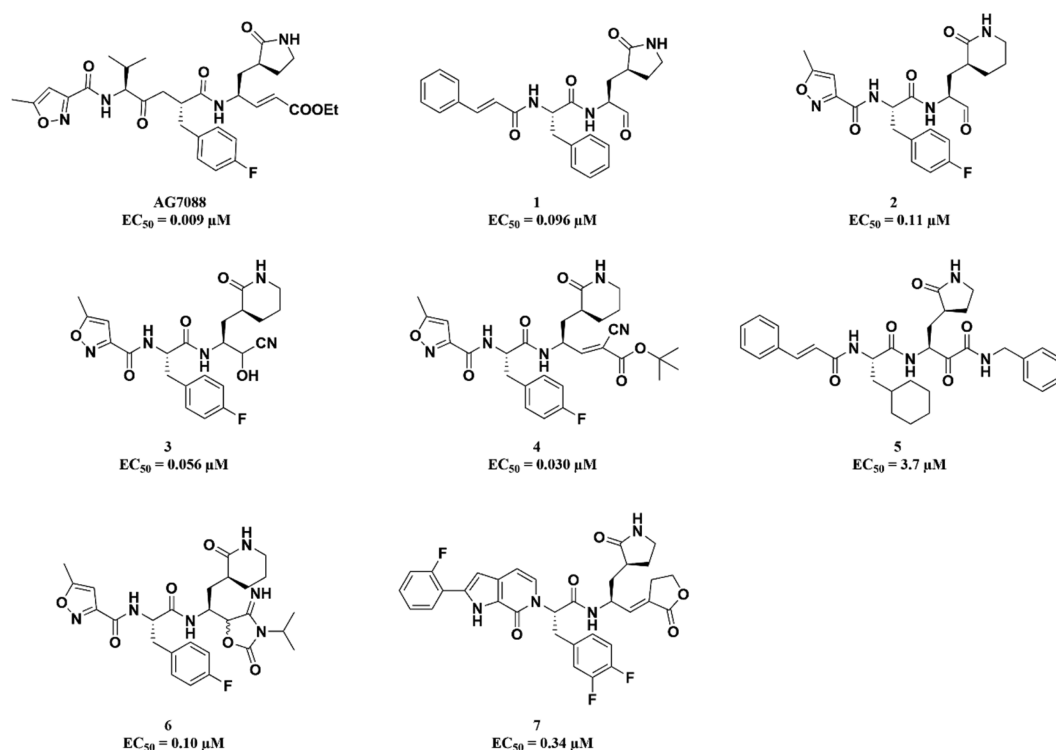


Figure 1. Representatives of reported EV71 3C protease inhibitors.

but its activity against coronaviruses is weak. Compounds 1^{5b} and 2^{5c,d} showed good anti-EV71 activity, and the selectivity of compounds 3^{5e} and 4^{5f} toward other common mammalian proteases was high, but their pharmaceutical properties were not satisfied; no more research progresses have been reported. Our compound (5^{5g}) exhibited broad-spectrum antiviral activity, but its activity against EV71 was weak. As reported, the plasma stability of compounds 6^{5h} and 7⁵ⁱ was impressive, while their pharmacokinetic properties needed to be further improved. Although many inhibitors with different warheads had been reported, there was still no effective drug on the market. With those in mind, novel broad-spectrum antiviral inhibitors with good pharmacokinetic properties and safety need to be designed.

RESULTS AND DISCUSSION

Compound Design. AG7088 has potent anti-EV71 activity (EC₅₀ = 0.009 μM), so we analyzed the crystal structure of EV71 3C^{Pro} with AG7088 (Figure 2) for our compound's design.⁶ The results demonstrate that α,β -unsaturated ester of AG7088 forms a covalent linkage with the Cys147 residue in the S1' subsite of

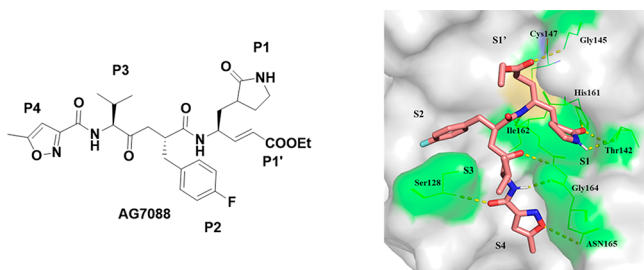


Figure 2. X-ray structure of the surface representation of EV71 3C^{Pro} (PDB ID: 4GHT) complexed with the AG7088 (yellow).

the EV71 3C^{Pro}, which is the key point for maintaining the antiviral activity. The (*S*)- γ -lactam ring at P1 position forms hydrogen bonds with the crucial residues including Thr142 and His161 in the S1 subsite, and the substituted phenyl group at the P2 position occupies the S2 subsite well. The complex also revealed that the isopropyl in the P3 moiety is solvent-exposed, and the P4 moiety forms hydrogen bonds with Gly164, Asn145, and Ser128.^{6h} Unfortunately, the α,β -unsaturated ester is easily hydrolyzed, the plasma stability of the AG7088 is poor, and its half-life in rat plasma is less than 2 min; in addition, AG7088 was inactive to the SARS-CoV 3CL protease (IC₅₀ > 100 μM).⁷ We want to overcome this shortcoming of AG7088 and obtain some novel compounds.

In our previous work, peptidomimetic α -ketoamides (compound 5) exhibited broad-spectrum antiviral activity.^{5g} Former reports showed that compound 1 also had good anti-EV71 activity (EC₅₀ = 0.096 μM). After analyzing the crystal structure of compound 1, compound 5, and AG7088, we found that they shared similar important key pharmacophore fragments with a warhead and (*S*)- γ -lactam ring. In this core structure, the warheads could be covalently linked to Cys147, and the lactam ring could interact with the crucial residues, and we envisioned AG7088 showed better antiviral activity might benefit from the additional interaction at the P3 and P4 position. When we embarked on designing the novel compounds (Figure 3), the key pharmacophore fragments in compounds 1, 5, and AG7088 were extracted, and then some common warheads were investigated to get compounds 19a and 19b. Subsequently, we introduced some heterocyclic moieties into the P3 position to obtain the corresponding peptidomimetic aldehydes 18b–18p. In a second approach, a valine moiety was introduced in the P3 position to keep the chain length similar to AG7088, and different heterocycles were investigated in the P4 position to get compounds 26a–26e.

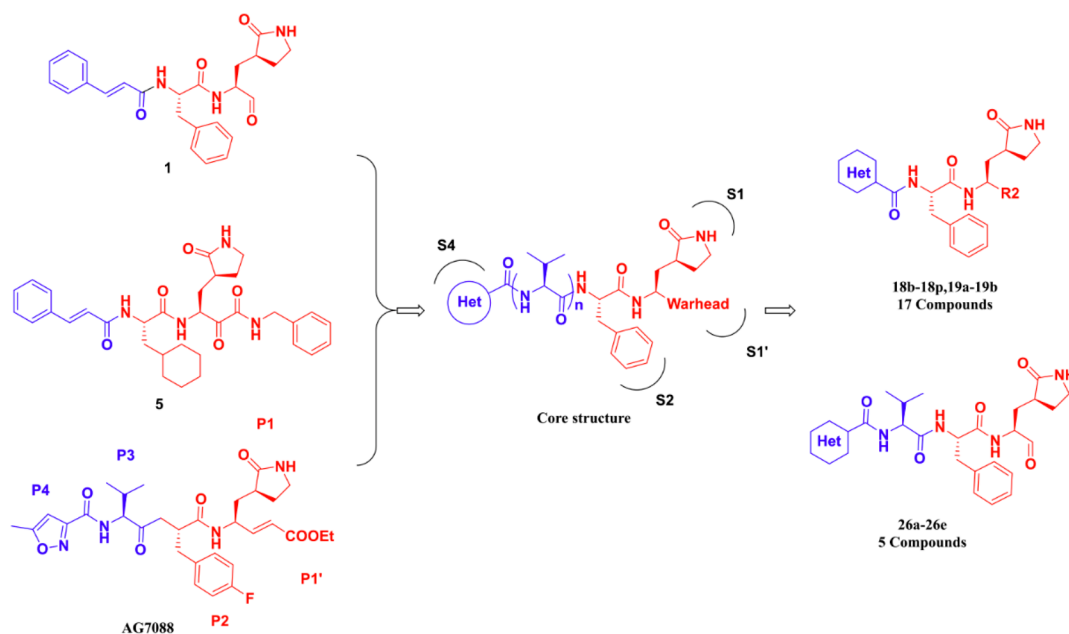
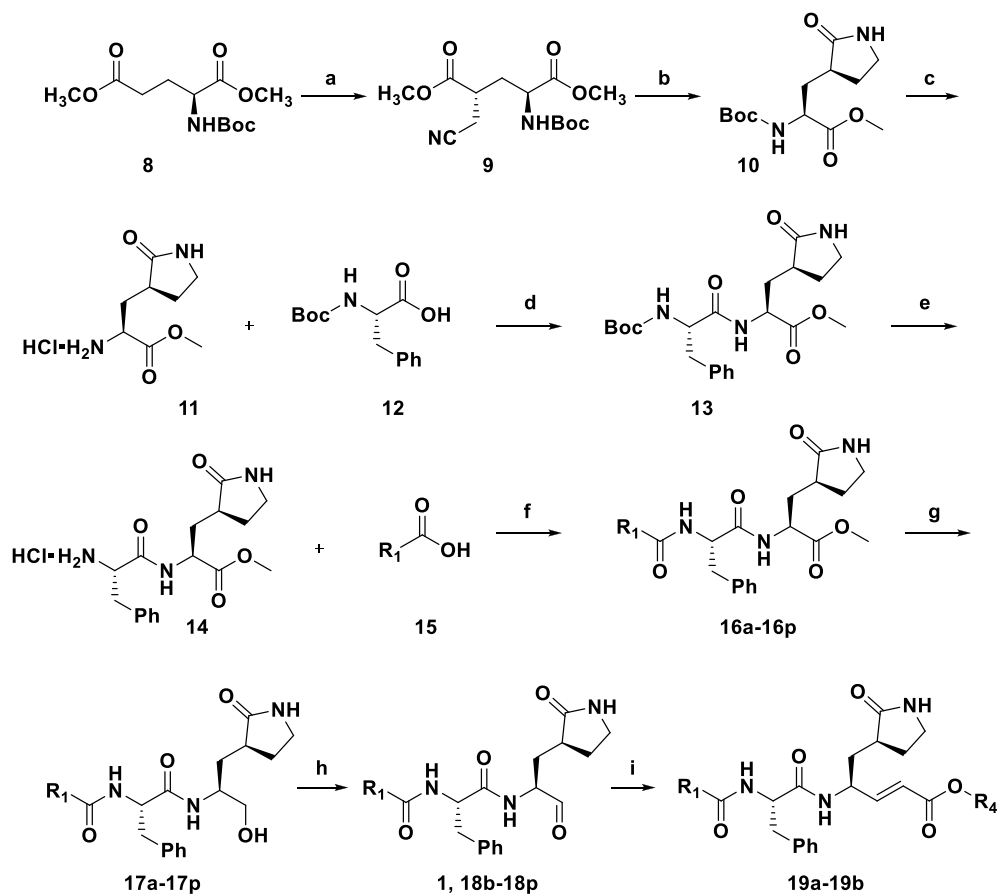


Figure 3. Design of novel EV71 3C protease inhibitors.

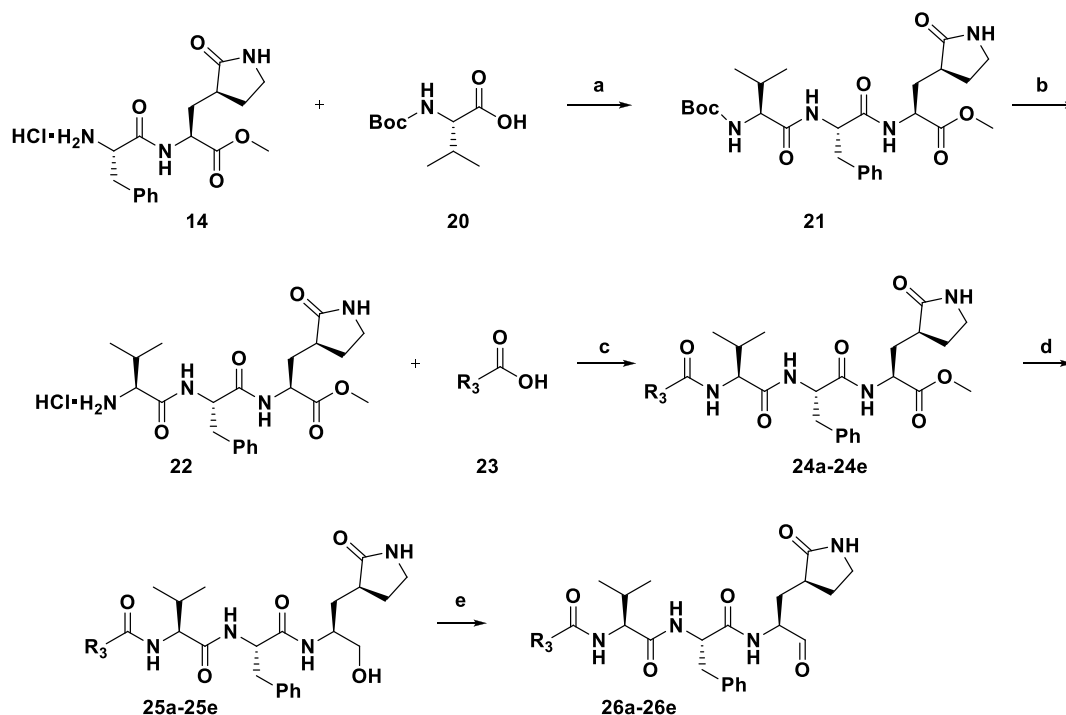
Scheme 1. Synthesis Procedure of Target Compounds^a



^aReagents and conditions: (a) LiHMDS, THF, -78°C ; (b) NaBH_4 , CoCl_2 , 0°C ; (c) 4 M HCl, 12 h; (d) HATU, DIPEA, CH_2Cl_2 , -20°C , 12 h; (e) 4 M HCl, 12 h; (f) HATU, DIPEA, CH_2Cl_2 , -20°C , 12 h; (g) NaBH_4 , CH_3OH ; (h) Dess–Martin periodinane, NaHCO_3 , CH_2Cl_2 ; (i) $\text{Ph}_3\text{PCH}_2\text{COOR}_4$, Et_3N , DCM.

Chemistry. The synthetic routes and chemical structures of the compounds (**19a**, **19b**, and **18b–18p**) are shown in [Scheme](#)

1. The starting material **8** was obtained from commercial suppliers and used without further purification, and the key

Scheme 2. Synthesis Procedure of Target Compounds^a

^aReagents and conditions: (a) HATU, DIPEA, CH₂Cl₂, -20 °C, 12 h; (b) 4 M HCl, 12 h; (c) HATU, DIPEA, CH₂Cl₂, -20 °C, 12 h; (d) NaBH₄, CH₃OH; (e) Dess–Martin Periodinane, NaHCO₃, CH₂Cl₂.

intermediate **11**^{5c} was synthesized by following the literature. The intermediate **13** was synthesized starting from the amino **11** and *N*-(*t*-butoxycarbonyl)-*L*-phenylalanine **12**. After the *t*-butoxycarbonyl group was removed from **13** by 4 M HCl in dioxane, the intermediate **14** was obtained. A subsequent coupling reaction between compound **14** and the corresponding acids **15** resulted in esters **16a–16p**. The peptidomimetic aldehydes **1** and **18b–18p** were approached via a two-step route, in which the ester derivatives **16a–16p** were first reduced with NaBH₄ to generate the primary alcohols **17a–17p**, and subsequently, **17a–17p** were oxidized into aldehydes **1** and **18b–18p** with Dess–Martin periodinane (DMP). Finally, compounds **19a** and **19b** were obtained from **1** by the Wittig reaction.

The synthetic procedure of compounds **26a–26e** was shown in Scheme 2. Compound **21** was obtained via a condensation reaction between the same intermediate **14** with *N*-(*t*-butoxycarbonyl)-*L*-valine **20**, and then, the *t*-butoxycarbonyl group of **21** was removed by 4 M HCl in dioxane to obtain **22**. Subsequently, compound **22** was coupled with the corresponding acid **23** to afford esters **24a–24e**. After completion of a reduction of the esters **24a–24e**, the desired products (**25a–25e**) were reoxidized by DMP to obtain the final products **26a–26e**.

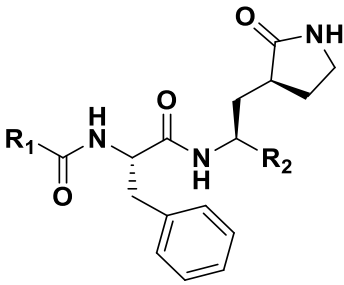
Structure–Activity Relationship of the Compounds.

All the synthesized compounds were tested for inhibitory activity of EV71 3C^{Pro} and antiviral activity of EV71, and results are summarized in Table 1 and Table 2.

Modification on R₁ and R₂. Structural modifications on R₁ and R₂ were first conducted, and a number of derivatives have been designed, synthesized, and biologically evaluated. The results were summarized in Table 1, and two compounds (compound **1** and AG7088) were used as references in this

work. IC₅₀ values of compound **1** were inconsistent with previous reports, which might be caused by a difference in enzyme concentration.^{5b} These data indicated that the enzyme inhibitory activity of peptidomimetic aldehyde (compound **1**, IC₅₀ = 4.57 ± 0.27 μM) was weaker than the compounds, in which α,β-unsaturated ester was defined as the warhead (compounds **19a** and **19b**), while compound **1** displayed better anti-EV71 activity (EC₅₀ = 0.10 ± 0.01 μM) than α,β-unsaturated methyl ester **19a** (EC₅₀ = 1.21 ± 0.14 μM) and α,β-unsaturated benzyl ester **19b** (EC₅₀ = 3.10 ± 0.09 μM), and the antiviral results showed that a small group might be more suitable in P1'. Based on the antiviral activity, an aldehyde was selected as a new warhead for further optimization. When aldehyde on R₂ was incorporated and the R₁ moiety was replaced with heterocyclic motifs, most of the target compounds (**18b–18l**, **18n**, and **18p**) showed better 3C^{Pro} inhibitory activity (IC₅₀ < 4.0 μM) than compound **1** (IC₅₀ = 4.57 μM), indicating that the introduction of the heterocyclic ring in P3 might be able to form additional interactions with the S4 subsite to improve the inhibitory activity of 3C^{Pro}. The inhibitory activity of compound **11m** was decreased, which might be due to the fact that the nitrogen atom in this compound could not form an additional interaction. As we know, the antiviral activity is a result caused by multiple factors, which was related not only to enzyme inhibitory activity but also the other properties such as permeability. So the EC₅₀ values deserved further discussion. The enzyme inhibitory activity of monocyclic moiety-substituted derivatives (**18b**, **18c**) was increased, while a lower antiviral activity was observed when comparing to compound **1**. Those results indicated that monocyclic moieties might not be a good choice on R₁, and then bicyclic heterocycles were investigated. The anti-EV71 activities of compounds with heterocyclic acene moieties **18d–18h** were decreased, and the

Table 1. Enzyme Inhibitory Activity and Anti-EV71 Activities of Peptidomimetic Aldehydes with R₁ and R₂ Modifications^a



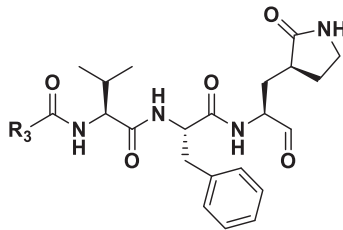
Compd.	R ₁	R ₂	IC ₅₀ (μM)	EC ₅₀ (μM)	CC ₅₀ (μM)
19a		CH=CHCOOCH ₃	1.73 ± 0.65	1.21 ± 0.14	>100
19b		CH=CHCOOBn	2.06 ± 0.04	3.10 ± 0.09	>100
18b		CHO	2.09 ± 0.18	0.32 ± 0.01	>100
18c		CHO	2.02 ± 0.24	0.47 ± 0.04	>100
18d		CHO	1.47 ± 0.15	0.22 ± 0.01	>100
18e		CHO	2.37 ± 0.31	0.29 ± 0.02	>100
18f		CHO	2.21 ± 0.31	0.30 ± 0.04	>100
18g		CHO	3.01 ± 0.07	0.77 ± 0.20	>100
18h		CHO	3.83 ± 0.52	0.69 ± 0.16	>100
18i		CHO	1.62 ± 0.01	0.36 ± 0.08	>100
18j		CHO	2.44 ± 0.22	0.093 ± 0.060	>100
18k		CHO	3.60 ± 0.38	0.14 ± 0.07	>100
18l		CHO	3.04 ± 0.17	0.37 ± 0.11	>100
18m		CHO	13.02 ± 1.25	0.12 ± 0.04	>100
18n		CHO	3.22 ± 0.17	0.094 ± 0.020	46.2
18o		CHO	4.34 ± 0.13	0.070 ± 0.010	16.4
18p		CHO	2.36 ± 1.01	0.030 ± 0.002	>100

^aEach value represented the average results from three independent experiments.

introduction of 7-bromoimidazo[1,2-*a*]pyridine (compound **18i**) also reduced the anti-EV71 activity. Subsequently, benzoheterocycles were introduced on R₁ (**18j**–**18p**), and compounds **18j**, **18k**, and **18m** had similar activities compared to compound **1**. The introduction of methyl on quinoxaline (**18l**) reduced the antiviral activity; when R₁ was replaced with a substituted quinoline (**18n**), the anti-EV71 activity was also increased. It was noteworthy that compound **18o** (EC₅₀ = 0.07 ± 0.01 μM) showed better anti-EV71 activity than compound **1**, albeit the cytotoxicity of these compounds was slightly increased (CC₅₀ = 16.4 μM). The 2-indole scaffold was incorporated, and the activity of **18p** against EV71 (EC₅₀ = 0.030 ± 0.002 μM) was increased. The discrepancy of the activities between compounds including **18h** and **18j** with **18p** indicated that the NH moiety in the 2-indole scaffold was vital for maintaining the anti-EV71 activity.

Modification on the R₃ Position. On the other hand, as showed in Table 2, structural modifications had been continued

Table 2. Enzyme Inhibitory Activity and anti-EV71 Activities of Peptidomimetic Aldehydes with R₃ Modifications^a



Compd.	R ₃	IC ₅₀ (μM)	EC ₅₀ (μM)	CC ₅₀ (μM)
26a		6.73 ± 0.60	0.090 ± 0.020	>100
26b		4.16 ± 0.19	0.12 ± 0.02	72.5
26c		2.43 ± 0.53	0.096 ± 0.040	>100
26d		7.49 ± 0.55	0.043 ± 0.010	82.8
26e		4.04 ± 0.25	0.44 ± 0.12	>100
1		4.57 ± 0.27	0.10 ± 0.01	>100
AG7088		1.89 ± 0.04	0.011 ± 0.007	>100

^aEach value represented the average results from three independent experiments.

by introducing a valine motif at the P3 position, and most of the target compounds (**26a**–**26e**) showed good enzyme inhibitory activities (ranging from 2.43 μM to 7.49 μM), while the inhibitory activities of those compounds were weaker than **AG7088** (IC₅₀ = 1.89 μM). We proposed the reason might be that, after replacing the carbon atom in **AG7088** with a nitrogen atom, the conformation of those compounds (**26a**–**26e**) changes a lot, which made those compounds unable to occupy the binding pocket very well, and α,β-unsaturated ester showed more potent inhibitory activity against 3C^{pro} than aldehyde. The results of antiviral activities showed that the introduction of 5-methyl-1,2-oxazolone and benzoheterocycles moiety on R₃ made the anti-EV71 activity of the corresponding compounds (**26a**–**26d**) comparable to compound **1**. Especially when the quinoline group was introduced into the R₃ position, compound **26d** showed good activity (EC₅₀ = 0.043 ± 0.010 μM), while the activities of these tripeptide compounds were decreased compared with compound **18p** and **AG7088**. In addition, compounds **26d** and **18p** exhibited safety cytotoxicity (CC₅₀ = 82.8 μM and CC₅₀ > 100 μM, respectively).

Crystal Structure of EV71 3C^{pro} in Complex with **18p**.

To understand the binding mode of these inhibitors with the protease, the complex structure of EV71 3C^{pro} bound with **18p** was determined at a resolution of 1.2 Å. Compound **18p** bound into the substrate-binding site at the surface of the protease and occupied S1, S2, and S4 subsites (Figure 4A). At the S1' subsite, the aldehyde group of **18p** covalently linked to the catalytic Cys147 of the protease (Figure 4B,C). In addition to this covalent bond, the oxygen atom of the aldehyde group established H-bonds with the side chain of catalytic His40 directly and the NH of the Gly145 main chain (part of the oxyanion hole) through a water molecule (Figure 4C). The (S)-γ-lactam ring of **18p** perfectly engaged within the S1 subsite. The oxygen atom of the (S)-γ-lactam ring formed H-bonds with the side chains of His161 and Thr142, while the nitrogen atom of

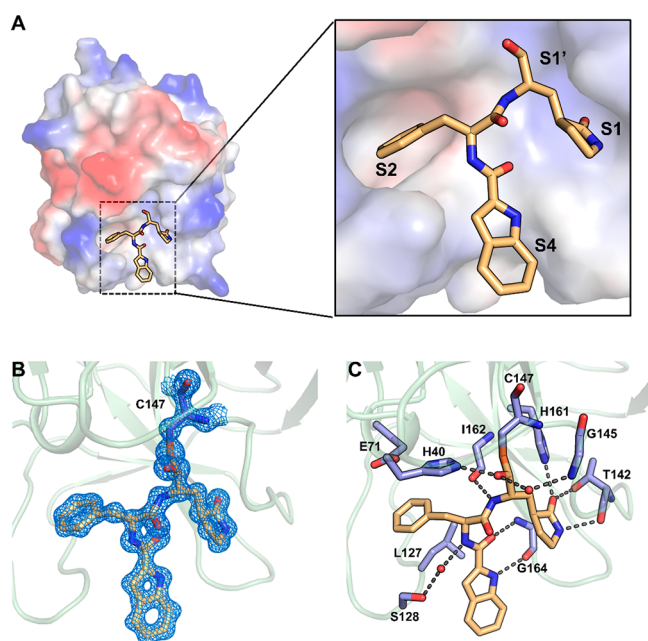


Figure 4. Crystal structure of the EV71 3C^{pro} in complex with **18p**. (A) The binding mode of **18p** at the substrate-binding site of the EV71 3C^{pro} (PDB code: 7DNC). The EV71 3C^{pro} was shown as a molecular surface, and **18p** was shown by light orange sticks. (B) 2Fo-Fc density maps contoured at 2.0 σ are shown for **18p** and C147. (C) Interactions of **18p** with the surrounding residues revealed by the crystal structure. Residues are shown as light blue sticks, and H-bonds are represented by black dashed lines.

the (*S*)- γ -lactam ring formed a H-bond with the main chain of Thr142. The benzyl ring of **18p** occupied the S2 subsite by forming hydrophobic interactions with His40, Glu71, and Leu127. The indole group of **18p** fitted into the S4 subsite and donated a H-bond to the main chain of Gly164. In addition, the amide bonds of **18p** also participated in binding by establishing H-bonds with Ile162 and Gly164 directly and with Ser128 through a water molecule (Figure 4C).

A structure overlay of the EV71 3C^{pro}-**18p** and the EV71 3C^{pro}-**AG7088** complexes revealed that these two compounds adopted similar binding modes (Figure S1A). The difference mainly lied in the interactions with the S1' and S4 subsites. **AG7088** covalently bound to the catalytic Cys147 with its α,β -unsaturated ketone, while the aldehyde group of **18p** was used to covalently link to the catalytic Cys147. Simultaneously, the oxygen atom of the aldehyde group participated in forming multiple H-bonds with the surrounding residues including the catalytic His40. At the S4 subsite, the indole ring of **18p** flipped up and established a shorter H-bond (2.9 Å) with Gly164 compared to the H-bond (3.1 Å) between **AG7088** and Gly164. In addition, a new H-bond was formed between the amide bond

of **18p** and Ser128, mediated by a water molecule (Figure S1B, C).

Activity on a Panel of Enteroviruses and Rhinoviruses.

Considering that the 3C proteases are conserved between different viruses, four compounds (**1**, **18p**, **19a**, and **26b**) were further tested against a panel of relevant enteroviruses and rhinoviruses, and results were summarized in Table 3. The results demonstrated that the derivatives with aldehyde warhead had potent broad-spectrum antiviral activities. Compound **1** showed better broad-spectrum antiviral activity than the α , β -unsaturated ester **19a**. Additionally, the dipeptide compound **18p** was proved to have more efficacy than the tripeptide compound **26b**. Besides, compounds **18p** also exhibited excellent anti-EV68 activity ($EC_{50} = 0.03 \pm 0.01 \mu\text{M}$), and compounds **18p** and **26b** also exhibited high anti-CoxA21 activity ($EC_{50} = 0.43 \pm 0.11 \mu\text{M}$ and $EC_{50} = 0.51 \pm 0.01 \mu\text{M}$, respectively), while its antiviral activities against CoxB3 and HRV were weak, which might be caused by the difference in substrate binding pockets (Figure S2). According to these results, compound **18p** has a lot of potential to be accessed in a broad-spectrum antiviral drug.

Antiviral Activity on SARS-CoV-2.

In late December 2019, an emerged coronavirus called SARS-CoV-2 (severe acute respiratory syndrome coronavirus 2), causes the pandemic COVID-19 (coronavirus disease 2019). There are no specific antiviral drugs approved by the FDA except Remdesivir, so the development of more effective antiviral drugs is of great significance.⁸ SARS-CoV-2 is an enveloped, positive-sense, single-stranded RNA virus that belongs to the β -lineage of the coronavirus. The genome is translated into two polyproteins, and then the polyproteins were cleaved by 3C-like protease (3CL^{pro}, also named the main protease) and papain-like proteinase (PL^{pro}). The majority of this proteolytic processing utilizes the 3CL^{pro}, which plays a vital role in SARS-CoV-2's replication. Unlike enterovirus 3C^{pro}, the active form of the SARS-CoV-2 3CL^{pro} is a dimer, and it has a catalytic dyad containing cysteine and histidine.^{9,10} As we know, the 3C^{pro} of EV71 and 3CL^{pro} of SARS-CoV-2 share some similarities; for example, both the catalytic sites contain cysteine and histidine, and a glutamine (Gln) is almost always required in the P1 position of their substrates. In our previous work, we found the active sites of 3C^{pro} and 3CL^{pro} also are similar and usually composed of four sites: S1', S1, S2, and S4.^{5g,9d} Recently, many inhibitors targeting SARS-CoV-2 3CL^{pro} have been reported, and most of them shared similar key pharmacophore fragments (warhead and lactam ring) and exhibited good inhibitor activity against 3CL^{pro} and replication of SARS-CoV-2 (Figure 5).^{9b,c,11} Among them, two peptide inhibitors developed by Pfizer (PF-007304814 is a phosphate prodrug of PF-00835231)^{11b} and our group (compound **29**)^{9d} show potent antiviral activity and good safety, and both have entered phase I clinical trials. Our antienterovirus compounds show some similarity to compound

Table 3. Activity of Inhibitors against a Panel of Enteroviruses and Rhinoviruses^a

compd	EV71 EC_{50} (μM)	EV68 EC_{50} (μM)	CoxA21 EC_{50} (μM)	CoxB3 EC_{50} (μM)	RV-A02-WT EC_{50} (μM)	RV-B14-WT EC_{50} (μM)
1	0.10 \pm 0.01	0.08 \pm 0.03	1.73 \pm 0.82	15.87	6.60	1.19
18p	0.030 \pm 0.002	0.03 \pm 0.01	0.43 \pm 0.11	4.19	1.62	0.81
19a	1.21 \pm 0.10	0.10 \pm 0.01	3.62 \pm 1.19	77.67	1.68	1.65
26b	0.12 \pm 0.02	0.26 \pm 0.10	0.51 \pm 0.01	9.15	1.02	0.98

^aThe value of EV71, EV68, and CoxA21 represented the average results from three independent experiments.

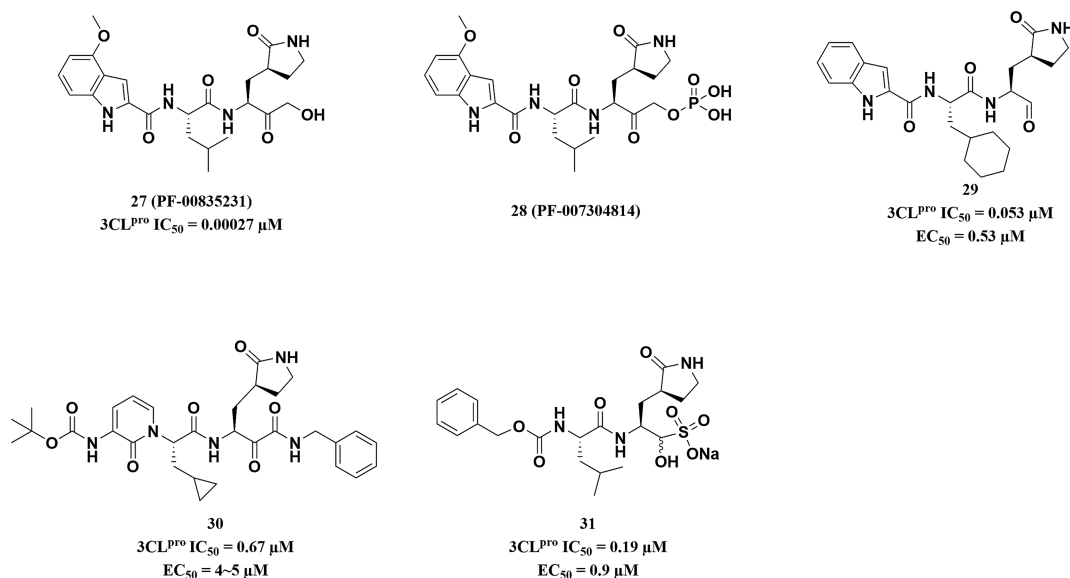


Figure 5. Representatives of reported SARS-CoV-2 3CL protease inhibitors

29, so some 3CL^{PRO} inhibitors were selected to be further tested against 3CL^{PRO} as well as the replication of SARS-CoV-2.

The results of enzyme inhibitory activity and anti-SARS-CoV-2 activity were summarized in Table 4. Most of the compounds

Table 4. Enzyme Inhibitory Activities and Anti-SARS-CoV-2 Activities of Peptidomimetic Aldehydes^a

compound	IC ₅₀ (μM)	EC ₅₀ (μM)	CC ₅₀ (μM)
18d	0.078 ± 0.016	1.35 ± 0.16	>1000
18e	0.059 ± 0.005	0.76 ± 0.26	>1000
18g	0.097 ± 0.017	8.21 ± 0.68	>1000
18j	0.080 ± 0.002	0.49 ± 0.001	>1000
18l	0.065 ± 0.011	0.44 ± 0.04	602.6
18m	0.140 ± 0.012	0.43 ± 0.05	627.2 ± 16.3
18n	0.240 ± 0.042	0.35 ± 0.03	823.1 ± 32.2
18o	0.120 ± 0.003	0.25 ± 0.04	298.7 ± 4.9
18p	0.034 ± 0.004	0.29 ± 0.06	808.7 ± 20.4
26a	0.067 ± 0.014	>2	>1000
26b	0.068 ± 0.012	4.22 ± 0.25	>1000
26c	0.067 ± 0.014	5.62 ± 1.26	>1000
26d	0.18 ± 0.029	4.12 ± 0.52	604.1 ± 5.9

^aEach value represented the average results from three independent experiments

showed excellent inhibitory activity of 3CL^{PRO} (IC₅₀ < 0.10 μM), especially when the IC₅₀ value of 18p was 0.034 μM. However, when the quinoline group was incorporated, the enzyme

inhibitory activities were decreased (18m, 18n, and 26d). In our previous work, the 2-indole moiety could form an additional H-bond with Glu166 in the S4 subsite.^{9d} When 2-quinoline and the derivative (18m, 18n, and 18o) were introduced, the H-bond could not be formed, so this might be the reason for the decrease of inhibitory activity against 3CL^{PRO}. Then, the antiviral activity against SARS-CoV-2 was evaluated, of which six benzoheterocyclic dipeptide compounds exhibited excellent inhibitory activity (EC₅₀ < 0.5 μM), and the EC₅₀ values of 18o and 18p were 0.25 μM and 0.29 μM, respectively. In addition, the selection index of 18p (SI = 2786) is better than 18o (SI = 1192). The results showed the inhibitory activities of the tripeptide compounds (26a–26d) were greater than 1 μM, and the reason might be that the tripeptide compounds showed poor membrane permeability.¹¹ Those results indicate the compound 18p also is a good starting point for further optimization as a SARS-CoV-2 inhibitor.

Preliminary Pharmacokinetic (PK) Evaluation of Compounds 18p and 26d. To explore the further druggability of the novel peptide aldehydes, compounds 18p and 26d were evaluated for their pharmacokinetic properties in mice after intraperitoneal (20 mg/kg), subcutaneous (5 mg/kg), and intravenous (5 mg/kg) administration. As shown in Table 5, compound 18p given intraperitoneally and subcutaneously displayed a much higher area under the curve (AUC) value than that of 26d. Compound 18p also displayed a longer half-life (*T*_{1/2}) of 5.85 h when administrated intravenously. Those results indicate that compound 18p has better PK properties than 26d

Table 5. Preliminary Pharmacokinetic (PK) Evaluation of Compounds 18p and 26d^a

compd	admin	<i>T</i> _{1/2} (h)	<i>T</i> _{max} (h)	<i>C</i> _{max} (ng/mL)	AUC _{int} (h ng/mL)	AUC _{INF_obs} (h ng/mL)	CL (mL/min/kg)	MRT (h)	V _{ss_obs} (mL/kg)	<i>F</i> (%)
18p	ip	5.36 ± 1.12	0.25	14572 ± 3105	15952 ± 3468	16080 ± 3559		1.69 ± 0.60		230
	sc	4.96 ± 0.71	0.58 ± 0.29	2762 ± 689	3568 ± 490	3579 ± 489		1.34 ± 0.21		206
	iv	5.85 ± 0.75			1732 ± 161	1745 ± 163	48.0 ± 4.7	1.42 ± 0.12	4119 ± 676	
26d	ip	5.38 ± 0.28	0.25	4542 ± 457	4637 ± 472	4651 ± 472		1.11 ± 0.01		84.2
	sc	5.03 ± 4.30	0.25	1159 ± 46	1321 ± 222	1338 ± 231		1.82 ± 0.89		96
	iv	2.98 ± 2.50			1378 ± 116	1390 ± 114	60.2 ± 4.7	0.98 ± 0.06	3536 ± 298	

^aThe value represented the average results from three independent experiments.

to warrant further study. The reason why the bioavailability of compound **18p** is greater than 100% may be due to changes in the clearance rate in different routes of administration, and the clearance rate of **18p** is fast by intravenous injection.¹²

CONCLUSION

In summary, a series of novel protease inhibitors with an aldehyde warhead was designed, synthesized, and biologically evaluated on EV71 by analyzing the crystal structure of EV71 3C protease with **AG7088**. Most of the compounds have potent inhibitory activity of 3C^{pro} and EV71. The SAR study indicated that the introduction of aldehyde at P1' position presented better antiviral activities than the α , β -unsaturated ester. Heteroaromatic scaffolds were introduced at the R₁ group, and most of the compounds displayed good antiviral activities, especially when R₁ is an indole moiety (**18p**). Compound **18p** not only has high inhibitory activity of 3C^{pro} and EV71 (3C^{pro}: IC₅₀ = 2.36 μ M, EV71: EC₅₀ = 0.030 μ M), but also against EV68 (EC₅₀ = 0.03 μ M), CoxA21 (EC₅₀ = 0.43 μ M) and RV-B14-WT (EC₅₀ = 0.81 μ M). It also showed moderate activity against CoxB3 (EC₅₀ = 4.19 μ M) and RV-A02-WT (EC₅₀ = 1.62 μ M) and low toxicity (CC₅₀ > 100 μ M). The crystal structure of EV71 3C^{pro} in complex with **18p** was also determined at a resolution of 1.2 Å. It showed that **18p** fitted into the S1', S1, S2, and S4 sites perfectly and established multiple H-bonds with the surrounding residues including the catalytic His40. In addition, the aldehyde group of **18p** covalently bound to the catalytic Cys147, which was essential for maintaining the potency of these newly designed inhibitors, and the NH in the indole group formed a hydrogen bond with the main chain of Gly164. Some compounds were further evaluated against 3CL^{pro} and SARS-CoV-2, and the **18p** also showed excellent inhibitory activity (3CL^{pro}: IC₅₀ = 0.034 μ M, SARS-CoV-2: EC₅₀ = 0.29 μ M). In addition, this class of compounds also has no reasons for concern regarding acute toxicity.^{9d} Compared with **AG7088**, compound **18p** exhibited good PK properties and more potent anticoronavirus activity, and it is an excellent starting point for further optimization toward a broad-spectrum antiviral drug.

EXPERIMENTAL SECTION

General Methods. The materials and solvents were purchased from commercial sources and used without further purification. All products were characterized by their NMR and MS spectra. ¹H and ¹³C NMR spectra were recorded on a 400, 500, or 600 MHz instrument. Compounds were purified by chromatography with silica gel (300–400 mesh). Analytical thin-layer chromatography (TLC) was HSGF 254 (0.15–0.2 mm thickness). Preparative thin-layer chromatography (PTLC) was HSGF 254 (0.4–0.5 mm thickness). High-resolution mass spectra (HRMS) were measured on a Micromass Ultra Q-TOF spectrometer. HPLC analysis of all final compounds was performed on Agilent-1100 HPLC with a binary pump and photodiode array detector (DAD), using an Agilent Extend-C18 column (150 mm \times 4.6 mm, 5 μ m). All final compounds were analyzed using MeOH/H₂O = 70:30 (v/v) (0.8 mL/min), and all of them had an at least 95% purity.

Synthetic Procedure of Compounds 9–11. The solution of lithium bis(trimethylsilyl)amide (LHMDS) (94 mL, 1 M in THF) was added dropwise to a solution of *N*-Boc-L-glutamic acid dimethyl ester (**8**) (12.0 g, 43.6 mmol) in THF (100 mL) at –78 °C; then, the mixture was stirred at –78 °C for 1 h. Subsequently, bromoacetonitrile (3.24 mL, 46.6 mmol) was added dropwise to the mixture under the temperature of –78 °C, and the reaction was kept at –78 °C for an additional 4 h. After the reactant was consumed, the reaction was quenched by NH₄Cl (40 mL). The reaction mixture was warm up to room temperature and extracted with ethyl acetate (50 mL \times 3). The organic layers were concentrated and

purified by flash column chromatography (petroleum ether/ethyl acetate = 4:1) to give product **9** (7.58 g, 55%) as a colorless oil. ¹H NMR (600 MHz, CDCl₃): δ 5.11 (d, *J* = 7.5 Hz, 1H), 4.38 (s, 1H), 3.77 (s, 3H), 3.75 (s, 3H), 2.92–2.82 (m, 1H), 2.81–2.71 (m, 2H), 2.24–2.08 (m, 2H), 1.44 (s, 9H).

Then, in a round-bottomed flask, compound **9** (6.0 g, 19.09 mmol) was dissolved in anhydrous MeOH (100 mL) before CoCl₂·6H₂O (2.72 g, 11.45 mmol) was added at 0 °C. Subsequently, NaBH₄ (4.35 g, 114.78 mmol) was added portionwise, and the reaction mixture was warmed to room temperature and stirred for 12 h. After the reactant was consumed, the reaction was quenched by NH₄Cl (30 mL). MeOH in the mixture was evaporated, and the residual mixture was extracted with ethyl acetate (50 mL \times 3). The organic layers were washed by saturated NH₄Cl solution (100 mL \times 3) and brine (100 mL \times 3); then, the organic phase was dried (MgSO₄) and concentrated. The residue was purified by flash column chromatography (petroleum ether/ethyl acetate = 2:1) to give product **10** (2.18 g, 40%) as a white solid. ¹H NMR (600 MHz, CDCl₃): δ 6.64 (s, 1H), 5.56 (s, 1H), 4.29 (d, *J* = 9.1 Hz, 1H), 3.71 (s, 3H), 3.37–3.26 (m, 2H), 2.47–2.42 (m, 2H), 2.13–2.08 (m, 1H), 1.84–1.81 (m, 2H), 1.41 (s, 9H).

Compound **10** (1.0 g, 3.5 mmol) was dissolved in 10 mL of DCM; then, the HCl (9 mL, 4 M in dioxane) was added. The reaction mixture was stirred at 20 °C for 12 h, and the mixture was concentrated in vacuo to get a white solid **11**, which could be used for the following step without purification.

Synthesis Procedure of Compound 13. To a solution of Boc-L-Phe-OH **12** (1.1 g, 3.5 mmol) in DCM (40 mL) was added HATU (1.9 g, 4.9 mmol) sequentially at –20 °C, and then the residue concentrated crude product **11** (0.77 g, 3.5 mmol) was added. After 30 min later, DIPEA (1.7 mL, 10.5 mmol) was added dropwise. Then, the reaction mixture was stirred at –20 °C for 12 h. The resulting mixture was washed by saturated ammonium chloride solution (100 mL \times 3), saturated NaHCO₃ solution (100 mL \times 3), and brine (100 mL \times 3). The organic phase layer was dried over Na₂SO₄ and concentrated in vacuo. The resulting mixture residue was purified by column chromatography (DCM/CH₃OH, 40:1 v/v) to afford the pure product **13** (1.26 g, 83%) as a light solid. ¹H NMR (400 MHz, CDCl₃): δ 7.61 (d, *J* = 7.0 Hz, 1H), 7.21 (m, 5H), 6.82 (s, 1H), 5.26 (s, 1H), 4.50 (d, *J* = 6.8 Hz, 2H), 3.69 (s, 3H), 3.36–3.25 (m, 2H), 3.12 (m, 1H), 2.99 (dd, *J* = 13.4, 7.3 Hz, 1H), 2.34 (s, 2H), 2.19–2.10 (m, 1H), 1.81 (m, 2H), 1.35 (s, 9H).

General Synthesis Procedure of Compounds 16a–16p. To a dry 100 mL flask in which **13** (1.5 g, 3.5 mmol) was dissolved with dry DCM was added 4 M HCl (9 mL, 35 mmol) slowly at 20 °C, and the resulting mixture was stirred at an ambient temperature for 12 h. The solvent was removed in vacuo, and the crude product **14** was directly used in the next step without further purification. Then, *trans*-3-phenylacrylic acid **15a** (0.49 g, 1.5 mmol) was dissolved in a dry 100 mL flask with CH₂Cl₂, HATU (0.68 g, 1.8 mmol) was added sequentially at –20 °C, and then compound **14** (0.55 g, 1.5 mmol) was added. DIPEA (0.73 mL, 4.5 mmol) was added dropwise after 30 min. Then, the reaction mixture was stirred at –20 °C for 12 h, followed by washing with a saturated ammonium chloride solution (100 mL \times 3), saturated NaHCO₃ solution (100 mL \times 3), and brine (100 mL \times 3). The organic phase was dried over Na₂SO₄ and concentrated, and the residue was purified by column chromatography (CH₂Cl₂/CH₃OH, 30:1 v/v) to afford the pure product **16a** (0.55 g, 80%) as a light solid. ¹H NMR (600 MHz, acetone-*d*₆): δ 8.45 (d, *J* = 7.4 Hz, 1H), 7.82 (d, *J* = 8.4 Hz, 1H), 7.54–7.47 (m, 3H), 7.37–7.31 (m, 5H), 7.26 (t, *J* = 7.6 Hz, 2H), 7.21–7.16 (m, 2H), 6.75 (d, *J* = 15.7 Hz, 1H), 5.01 (td, *J* = 8.4, 5.1 Hz, 1H), 4.53 (m, 1H), 3.69 (s, 3H), 3.33–3.24 (m, 3H), 3.04 (dd, *J* = 13.9, 8.5 Hz, 1H), 2.46 (dd, *J* = 9.8, 4.7 Hz, 1H), 2.31 (dd, *J* = 7.4, 4.8 Hz, 1H), 2.24–2.15 (m, 1H), 1.79 (m, 2H).

General Synthesis Procedure of Compounds 17a–17p. In a dry 100 mL flask was dissolved **16a** (0.92 g, 2.0 mmol) in dry THF, NaBH₄ (0.6 g, 16 mmol) was added slowly at 0 °C, and then, the reaction mixture was stirred at rt for 3 h. The completion of the reaction was confirmed by TLC; then the reaction was quenched and concentrated to get a crude residue. The residue was dissolved in DCM and washed with saturated ammonium chloride solution (50 mL \times 3), saturated

NaHCO₃ solution (50 mL × 3), and brine (50 mL × 3). The organic phase was dried over Na₂SO₄ and concentrated, and the residue was purified by column chromatography (DCM/CH₃OH, 20:1 v/v) to afford the pure product **17a** (0.77 g, 90%) as a light solid. ¹H NMR (500 MHz, methanol-*d*₄): δ 7.97 (d, *J* = 8.8 Hz, 1H), 7.55–7.48 (m, 3H), 7.40–7.34 (m, 3H), 7.32–7.28 (m, 4H), 7.23 (td, *J* = 6.0, 3.2 Hz, 2H), 6.67 (d, *J* = 15.8 Hz, 1H), 4.74 (dd, *J* = 8.1, 6.7 Hz, 1H), 3.98–3.91 (m, 1H), 3.44 (dd, *J* = 11.0, 5.0 Hz, 1H), 3.34–3.22 (m, 4H), 3.17 (dd, *J* = 13.7, 6.6 Hz, 1H), 3.05 (dd, *J* = 13.7, 8.3 Hz, 1H), 2.46 (dd, *J* = 9.8, 2.5 Hz, 1H), 2.37–2.27 (m, 1H), 1.98–1.89 (m, 1H), 1.81–1.69 (m, 1H), 1.55 (m, 1H).

General Synthesis Procedure of Compounds 1 and 18b–18p. To a solution of the **17a** (0.87 g, 2.0 mmol) in CH₂Cl₂ was added DMP (1.01 g, 2.4 mmol) slowly, and the reaction mixture was stirred at room temperature for 5 h. The completion of the reaction was confirmed by TLC, the reaction was quenched and concentrated, and the reaction was filtered and washed with saturated NaHCO₃ solution (50 mL × 3) and brine (50 mL × 3). The organic phase was dried over Na₂SO₄ and concentrated, and the residue was purified by column chromatography (DCM/CH₃OH, 20:1 v/v) to afford the pure product **1** (0.65 g, 76%) as a light solid. ¹H NMR (500 MHz, acetone-*d*₆): δ 9.38 (s, 1H), 7.57 (dt, *J* = 10.6, 8.4 Hz, 4H), 7.42–7.36 (m, 3H), 7.34–7.25 (m, 4H), 7.22 (d, *J* = 6.7 Hz, 1H), 6.84 (s, 1H), 6.80–6.72 (m, 1H), 4.90 (dd, *J* = 7.9, 5.7 Hz, 1H), 4.54–4.19 (m, 1H), 4.06–3.80 (m, 1H), 3.29–3.16 (m, 3H), 3.11 (m, 1H), 2.40–2.17 (m, 2H), 1.97 (dd, *J* = 14.1, 3.8 Hz, 1H), 1.82–1.48 (m, 2H).

General Synthesis Procedure of Compounds 19a and 19b. To a solution of the **1** (0.86 g, 2.0 mmol) in CH₂Cl₂ were added methyl-(triphenylphosphoranyl)idene acetate (0.80 g, 2.4 mmol) and Et₃N (0.56 mL, 4 mmol); then the reaction mixture was stirred at room temperature for 12 h. The completion of the reaction was confirmed by TLC; then the reaction was washed with saturated ammonium chloride solution (50 mL × 3), saturated NaHCO₃ solution (50 mL × 3), and brine (50 mL × 3). The organic phase was dried over Na₂SO₄ and concentrated, and the residue was purified by column chromatography (DCM/CH₃OH, 40:1 v/v) to afford the pure product **19a** (0.78 g, 78%) as a light solid.

Synthesis Procedure of Compound 21. To a solution of Boc-L-Val-OH **20** (0.76 g, 3.5 mmol) in DCM (40 mL) was added HATU (1.9 g, 4.9 mmol) sequentially at –20 °C, and then the residue concentrated crude product **14** (1.28 g, 3.5 mmol) was added. After 30 min later, DIPEA (1.7 mL, 10.5 mmol) was added dropwise. Then, the reaction mixture was stirred at –20 °C for 12 h. The resulting mixture was washed by saturated ammonium chloride solution (100 mL × 3), saturated NaHCO₃ solution (100 mL × 3), and brine (100 mL × 3). The organic phase layer was dried over Na₂SO₄ and concentrated in vacuo. The resulting mixture residue was purified by column chromatography (DCM/CH₃OH, 40:1 v/v) to afford the pure product **21** (1.58 g, 85%) as a light solid. ¹H NMR (600 MHz, CDCl₃): δ 7.67 (d, *J* = 7.7 Hz, 1H), 7.49 (d, *J* = 8.5 Hz, 1H), 7.24–7.14 (m, 6H), 7.01 (s, 1H), 5.11 (d, *J* = 9.1 Hz, 1H), 4.97–4.91 (m, 1H), 4.52 (t, *J* = 8.1 Hz, 1H), 3.84 (t, *J* = 8.1 Hz, 1H), 3.66 (s, 3H), 3.31 (m, 2H), 3.07 (d, *J* = 5.9 Hz, 2H), 2.39–2.27 (m, 1H), 2.18–2.06 (m, 2H), 1.99 (dd, *J* = 13.6, 6.8 Hz, 1H), 1.80–1.71 (m, 2H), 1.43 (s, 9H), 0.87 (d, *J* = 6.6 Hz, 3H), 0.82 (d, *J* = 6.6 Hz, 3H).

General Synthesis Procedure of Compounds 24a–24e. To a dry 100 mL flask in which **21** (1.86 g, 3.5 mmol) was dissolved in dry DCM was added 4 M HCl (9 mL, 35 mmol) slowly at 20 °C, and the resulting mixture was stirred at an ambient temperature for 12 h. The solvent was removed in vacuo, and the crude product **22** was directly used in next step without further purification. Then compound **22** was coupled with quinaldic acid **23d** to get the esters **24d** (0.96 g, 80%), and the synthesis procedure is similar to **17a**. ¹H NMR (400 MHz, CDCl₃): δ 8.60 (d, *J* = 9.5 Hz, 1H), 8.31 (d, *J* = 8.5 Hz, 1H), 8.25 (d, *J* = 8.5 Hz, 1H), 8.11 (d, *J* = 8.5 Hz, 1H), 7.97–7.86 (m, 2H), 7.81–7.75 (m, 1H), 7.72 (d, *J* = 8.4 Hz, 1H), 7.67–7.59 (m, 1H), 7.27 (s, 1H), 7.16 (d, *J* = 7.3 Hz, 2H), 7.02 (t, *J* = 7.6 Hz, 2H), 6.81 (t, *J* = 7.4 Hz, 1H), 5.00 (td, *J* = 8.3, 5.1 Hz, 1H), 4.64 (ddd, *J* = 11.6, 8.4, 3.2 Hz, 1H), 4.39 (dd, *J* = 9.2, 8.2 Hz, 1H), 3.69 (s, 3H), 3.40 (t, *J* = 8.6 Hz, 2H), 3.18 (dd, *J* = 13.8, 5.0 Hz, 1H),

3.01 (dd, *J* = 13.8, 8.0 Hz, 1H), 2.49–2.40 (m, 1H), 2.23 (m, 3H), 1.92–1.77 (m, 2H), 1.00 (d, *J* = 6.7 Hz, 3H), 0.95 (d, *J* = 6.7 Hz, 3H).

General Synthesis Procedure of Compounds 25a–25e. In a dry 100 mL flask was dissolved the **24d** (0.88 g, 1.5 mmol) in dry THF, NaBH₄ (0.45 g, 12 mmol) was added slowly at 0 °C, and then the reaction mixture was stirred at rt for 3 h. The completion of the reaction was confirmed by TLC; then the reaction was quenched and concentrated to get a crude residue. The residue was dissolved in DCM and washed with saturated ammonium chloride solution (50 mL × 3), saturated NaHCO₃ solution (50 mL × 3), and brine (50 mL × 3). The organic phase was dried over Na₂SO₄ and concentrated, and the residue was purified by column chromatography (DCM/CH₃OH, 20:1 v/v) to afford the pure product **25d** (0.71 g, 85%) as a light solid. ¹H NMR (400 MHz, CDCl₃): δ 8.60 (d, *J* = 8.3 Hz, 1H), 8.18 (d, *J* = 8.5 Hz, 1H), 8.09 (d, *J* = 8.5 Hz, 1H), 7.93 (t, *J* = 8.1 Hz, 2H), 7.84 (d, *J* = 7.7 Hz, 1H), 7.65 (t, *J* = 7.1 Hz, 1H), 7.62–7.52 (m, 2H), 7.19 (d, *J* = 7.3 Hz, 2H), 7.09 (t, *J* = 7.6 Hz, 2H), 7.02–6.87 (m, 2H), 4.91 (dd, *J* = 14.4, 8.4 Hz, 1H), 4.45 (dd, *J* = 8.0, 6.7 Hz, 1H), 4.10–3.98 (m, 1H), 3.57 (ddd, *J* = 33.4, 11.4, 4.6 Hz, 2H), 3.43–3.23 (m, 3H), 3.17 (dd, *J* = 13.7, 5.7 Hz, 1H), 3.02 (dd, *J* = 13.7, 8.4 Hz, 1H), 2.35 (m, 3H), 2.16–2.00 (m, 1H), 1.78 (dd, *J* = 11.5, 9.3 Hz, 1H), 1.57 (m, 1H), 0.97 (d, *J* = 6.7 Hz, 3H), 0.92 (d, *J* = 6.8 Hz, 3H).

General Synthesis Procedure of Compounds 26a–26e. To a solution of the **25d** (0.56 g, 1.0 mmol) in CH₂Cl₂ was added DMP (0.51 g, 1.2 mmol) slowly, and the reaction mixture was stirred at room temperature. The completion of the reaction was confirmed by TLC; then, the reaction was quenched and concentrated, and the reaction was filtered and washed with saturated NaHCO₃ solution (50 mL × 3) and brine (50 mL × 3). The organic phase was dried over Na₂SO₄ and concentrated, and the residue was purified by column chromatography (DCM/CH₃OH, 20:1 v/v) to afford the pure product **26d** (0.42 g, 76%) as a light solid.

Methyl (S,E)-4-((S)-2-Cinnamamido-3-phenylpropanamido)-5-((S)-2-oxopyrrolidin-3-yl)pent-2-enoate (19a). ¹H NMR (500 MHz, acetone-*d*₆): δ 8.15 (d, *J* = 8.2 Hz, 1H), 7.99 (d, *J* = 8.1 Hz, 1H), 7.77–7.61 (m, 1H), 7.55 (s, 1H), 7.52 (dd, *J* = 6.7, 2.6 Hz, 2H), 7.39–7.34 (m, 3H), 7.31 (d, *J* = 7.2 Hz, 2H), 7.26 (t, *J* = 7.6 Hz, 3H), 7.21–7.18 (m, 1H), 7.15 (s, 1H), 6.86 (dd, *J* = 15.7, 5.3 Hz, 1H), 6.80 (d, *J* = 15.8 Hz, 1H), 5.83 (dd, *J* = 15.7, 1.6 Hz, 1H), 4.96 (dd, *J* = 14.8, 7.6 Hz, 1H), 4.75–4.68 (m, 1H), 3.69 (s, 3H), 3.26–3.22 (m, 1H), 3.11 (dd, *J* = 13.6, 7.6 Hz, 1H), 2.30–2.23 (m, 1H), 2.05–1.97 (m, 2H), 1.80–1.73 (m, 1H), 1.61 (td, *J* = 9.7, 4.9 Hz, 1H); ¹³C NMR (125 MHz, acetone-*d*₆): δ 179.4, 171.4, 166.2, 165.4, 148.5, 140.0, 137.5, 135.2, 132.0, 131.9, 131.8, 129.4, 128.8, 128.7, 128.6, 128.3, 127.7, 126.6, 121.6, 120.1, 55.2, 50.8, 48.5, 40.0, 38.0, 35.2. HRMS (ESI) *m/z*: [M – H][–] calcd for C₂₈H₃₀N₃O₅, 488.2191; found, 488.2182. Purity: 98.6%.

Benzyl (S,E)-4-((S)-2-Cinnamamido-3-phenylpropanamido)-5-((S)-2-oxopyrrolidin-3-yl)pent-2-enoate (19b). ¹H NMR (600 MHz, CDCl₃): δ 7.90 (s, 1H), 7.55 (dd, *J* = 15.6, 2.7 Hz, 1H), 7.47–7.41 (m, 2H), 7.40–7.29 (m, 9H), 7.19 (d, *J* = 4.1 Hz, 4H), 7.10 (m, 1H), 6.92 (s, 1H), 6.72 (dd, *J* = 15.6, 5.4 Hz, 2H), 6.47 (d, *J* = 15.6 Hz, 1H), 5.76 (d, *J* = 15.7 Hz, 1H), 5.15 (s, 2H), 5.08 (d, *J* = 6.7 Hz, 1H), 4.49 (d, *J* = 5.3 Hz, 1H), 3.25 (m, 2H), 3.19–3.13 (m, 1H), 3.07 (dd, *J* = 13.5, 7.2 Hz, 1H), 2.27 (s, 2H), 1.95 (t, *J* = 10.8 Hz, 1H), 1.73–1.62 (m, 1H), 1.54–1.47 (m, 1H), 1.26 (d, *J* = 1.3 Hz, 1H). ¹³C NMR (150 MHz, CDCl₃): δ 179.7, 170.9, 165.6, 147.1, 141.2, 135.9, 135.5, 134.2, 129.4, 129.1, 128.4, 128.2, 128.1, 127.5, 126.6, 120.5, 119.9, 66.0, 54.1, 48.8, 48.7, 40.3, 38.7, 37.9, 34.4, 28.0. HRMS (ESI) *m/z*: [M – H][–] calcd for C₃₄H₃₄N₃O₅, 564.2504; found, 564.2508. Purity: 98.1%.

5-Methyl-N-((S)-1-oxo-3-((S)-2-oxopyrrolidin-3-yl)propan-2-yl)amino)-3-phenylpropan-2-yl)isoxazole-3-carboxamide (18b). ¹H NMR (600 MHz, acetone-*d*₆): δ 11.14 (d, *J* = 8.4 Hz, 1H), 9.41 (s, 1H), 8.28–8.23 (m, 1H), 7.78 (dd, *J* = 12.5, 8.8 Hz, 1H), 7.58 (d, *J* = 1.8 Hz, 1H), 7.47 (d, *J* = 8.8 Hz, 1H), 7.37–7.33 (m, 2H), 7.23 (d, *J* = 7.7 Hz, 2H), 7.16 (dd, *J* = 6.3, 1.9 Hz, 4H), 5.44 (dd, *J* = 70.6, 8.0 Hz, 1H), 5.06 (dd, *J* = 7.1, 4.5 Hz, 1H), 4.51 (m, 1H), 4.13–3.99 (m, 1H), 3.32 (d, *J* = 2.0 Hz, 1H), 3.20 (m, 2H), 2.44–2.34 (m, 1H), 2.33–2.25 (m, 1H), 1.79–1.55 (m, 2H). ¹³C NMR (125 MHz, acetone-*d*₆): δ 199.6, 179.0, 171.0, 170.8, 158.3, 136.8, 129.0, 127.9, 126.2, 100.7, 57.0, 54.0, 39.6, 37.4, 29.3, 27.6, 10.8. HRMS (ESI) *m/z*:

$[M - H]^-$ calcd for $C_{21}H_{23}N_4O_5$, 411.1674; found, 411.1682. Purity: 95.0%.

5-Fluoro-N-((S)-1-oxo-1-(((S)-1-oxo-3-((S)-2-oxopyrrolidin-3-yl)propan-2-yl)amino)-3-phenylpropan-2-yl)picolinamide (18c). 1H NMR (600 MHz, acetone- d_6): δ 9.42 (s, 1H), 8.87 (d, $J = 12.0$ Hz, 1H), 8.75 (d, $J = 6.0$ Hz, 1H), 8.63 (d, $J = 2.7$ Hz, 1H), 8.24 (d, $J = 8.1$ Hz, 1H), 7.98–7.94 (m, 1H), 7.37 (d, $J = 7.3$ Hz, 2H), 7.30 (dd, $J = 10.4, 4.7$ Hz, 2H), 7.22 (m, 1H), 5.01 (m, 1H), 4.32–4.27 (m, 1H), 3.38–3.34 (m, 1H), 3.31–3.27 (m, 1H), 3.19 (dd, $J = 13.9, 8.9$ Hz, 1H), 2.51–2.40 (m, 1H), 2.39–2.33 (m, 1H), 1.97–1.88 (m, 1H), 1.82 (m, 1H), 1.39 (s, 1H), 1.31 (d, $J = 2.5$ Hz, 2H). ^{13}C NMR (150 MHz, acetone- d_6): δ 200.1, 179.3, 171.7, 163.9, 160.0, 158.3, 144.7, 140.3, 137.7, 129.4, 128.3, 126.6, 121.7, 58.0, 55.3, 40.1, 38.2, 37.6, 30.8. HRMS (ESI) m/z : $[M - H]^-$ calcd for $C_{22}H_{22}FN_4O_4$, 425.1631; found, 425.1631. Purity: 95.7%.

N-((S)-1-Oxo-1-(((S)-1-oxo-3-((S)-2-oxopyrrolidin-3-yl)propan-2-yl)amino)-3-phenylpropan-2-yl)benzo[d][1,3]dioxole-5-carboxamide (18d). 1H NMR (500 MHz, $CDCl_3$): δ 9.25 (s, 1H), 8.47 (d, $J = 6.3$ Hz, 1H), 7.32–7.20 (m, 8H), 6.89 (s, 1H), 6.78–6.73 (m, 1H), 5.97 (s, 2H), 5.16–4.92 (m, 1H), 4.44–4.24 (m, 1H), 3.31–3.21 (m, 3H), 2.33 (m, 2H), 2.03–1.45 (m, 3H). ^{13}C NMR (125 MHz, $CDCl_3$): δ 199.9, 180.0, 172.4, 166.5, 150.5, 147.8, 136.6, 129.5, 128.5, 127.9, 126.9, 122.1, 107.9, 107.7, 101.7, 57.7, 54.6, 40.6, 38.8, 38.0, 29.7, 28.4. HRMS (ESI) m/z : $[M - H]^-$ calcd for $C_{24}H_{24}N_3O_6$, 450.1671; found, 450.1663. Purity: 96.7%.

N-((S)-1-Oxo-1-(((S)-1-oxo-3-((S)-2-oxopyrrolidin-3-yl)propan-2-yl)amino)-3-phenylpropan-2-yl)benzofuran-5-carboxamide (18e). 1H NMR (500 MHz, acetone- d_6): δ 9.43 (s, 1H), 8.59 (d, $J = 6.8$ Hz, 1H), 8.18 (dd, $J = 15.6, 1.8$ Hz, 1H), 8.08–7.99 (m, 1H), 7.92–7.82 (m, 2H), 7.53 (t, $J = 8.1$ Hz, 1H), 7.38 (d, $J = 7.3$ Hz, 2H), 7.28 (t, $J = 7.5$ Hz, 2H), 7.19 (t, $J = 7.3$ Hz, 1H), 7.13 (s, 1H), 6.97–6.90 (m, 1H), 5.07 (m, 1H), 4.37 (m, 1H), 3.37–3.33 (m, 1H), 3.29–3.20 (m, 3H), 2.52–2.24 (m, 2H), 2.05–1.98 (m, 1H), 1.87–1.62 (m, 2H). ^{13}C NMR (125 MHz, acetone- d_6): δ 200.1, 179.3, 172.3, 166.9, 156.5, 146.7, 137.9, 129.5, 128.3, 127.4, 126.5, 124.1, 121.1, 110.8, 107.1, 57.6, 55.3, 40.0, 37.9, 37.8. HRMS (ESI) m/z : $[M - H]^-$ calcd for $C_{25}H_{24}N_3O_5$, 446.1721; found, 446.1715. Purity: 95.2%.

N-((S)-1-Oxo-1-(((S)-1-oxo-3-((S)-2-oxopyrrolidin-3-yl)propan-2-yl)amino)-3-phenylpropan-2-yl)-2,3-dihydrobenzo[b][1,4]dioxine-6-carboxamide (18f). 1H NMR (500 MHz, $CDCl_3$): δ 9.22 (s, 1H), 8.36 (d, $J = 6.3$ Hz, 1H), 7.32 (d, $J = 2.0$ Hz, 1H), 7.23 (s, 5H), 7.02 (d, $J = 8.1$ Hz, 1H), 6.83 (d, $J = 8.4$ Hz, 1H), 6.55 (s, 1H), 5.07 (m, 1H), 4.27–4.21 (m, 6H), 3.31–3.24 (m, 2H), 3.20 (dd, $J = 14.4, 6.7$ Hz, 2H), 2.35–2.28 (m, 2H), 1.90 (dd, $J = 10.2, 6.4$ Hz, 1H), 1.80 (m, 2H). ^{13}C NMR (125 MHz, $CDCl_3$): δ 200.0, 180.0, 172.3, 166.4, 146.7, 143.3, 136.5, 129.5, 128.5, 127.0, 120.7, 117.2, 116.7, 64.5, 64.2, 57.7, 54.5, 40.6, 38.8, 38.0, 29.5, 28.5. HRMS (ESI) m/z : $[M - H]^-$ calcd for $C_{25}H_{26}N_3O_6$, 464.1827; found, 464.1824. Purity: 97.5%.

N-((S)-1-Oxo-1-(((S)-1-oxo-3-((S)-2-oxopyrrolidin-3-yl)propan-2-yl)amino)-3-phenylpropan-2-yl)-2,3-dihydrobenzo[b][1,4]dioxine-5-carboxamide (18g). 1H NMR (600 MHz, acetone- d_6): δ 11.14 (d, $J = 8.8$ Hz, 1H), 9.41 (s, 1H), 8.28–8.23 (m, 1H), 7.78 (m, 1H), 7.58 (d, $J = 1.8$ Hz, 1H), 7.47 (d, $J = 8.8$ Hz, 1H), 7.37–7.33 (m, 2H), 7.23 (d, $J = 7.7$ Hz, 2H), 7.16 (dd, $J = 6.3, 1.9$ Hz, 4H), 5.44 (m, 1H), 5.06 (dd, $J = 7.1, 4.5$ Hz, 1H), 4.51 (m, 1H), 4.13–3.99 (m, 1H), 3.32 (d, $J = 2.0$ Hz, 1H), 3.20 (m, 2H), 2.44–2.34 (m, 1H), 2.33–2.25 (m, 1H), 1.79–1.55 (m, 2H). ^{13}C NMR (125 MHz, acetone- d_6): δ 199.8, 178.9, 171.4, 163.7, 143.5, 142.2, 136.8, 129.2, 127.9, 126.3, 122.8, 121.6, 120.3, 97.9, 64.5, 63.3, 57.1, 54.5, 53.4, 39.6, 37.4, 27.7. HRMS (ESI) m/z : $[M - H]^-$ calcd for $C_{25}H_{26}N_3O_6$, 464.1827; found, 464.183. Purity: 97.6%.

N-((R)-1-Oxo-1-(((R)-1-oxo-3-((R)-2-oxopyrrolidin-3-yl)propan-2-yl)amino)-3-phenylpropan-2-yl)-1H-indole-5-carboxamide (18h). 1H NMR (500 MHz, acetone- d_6): δ 10.53 (s, 1H), 9.39 (s, 1H), 8.19–8.16 (m, 1H), 7.73 (d, $J = 8.0$ Hz, 1H), 7.66 (dd, $J = 8.5, 1.7$ Hz, 1H), 7.43 (d, $J = 8.5$ Hz, 1H), 7.40–7.38 (m, 1H), 7.37–7.33 (m, 2H), 7.26 (m, 2H), 7.19–7.15 (m, 1H), 6.96 (s, 1H), 6.54 (m, 1H), 5.01 (dt, $J = 8.2, 4.0$ Hz, 1H), 4.31–4.26 (m, 1H), 3.31 (dd, $J = 8.2, 5.6$ Hz, 1H), 3.26–3.18 (m, 3H), 2.45–2.36 (m, 1H), 2.32–2.21 (m, 1H), 1.98–1.95 (m, 1H), 1.81–1.68 (m, 2H). ^{13}C NMR (125 MHz, acetone- d_6): δ 199.7, 178.6, 171.9, 167.3, 137.6, 137.5, 129.0, 127.8, 127.2, 126.0,

125.8, 125.1, 120.4, 119.9, 110.4, 102.1, 57.1, 54.6, 39.5, 37.4. HRMS (ESI) m/z : $[M - H]^-$ calcd for $C_{25}H_{25}N_4O_4$, 445.1881; found, 445.1873. Purity: 95.1%.

6-Bromo-N-((S)-1-oxo-1-(((S)-1-oxo-3-((S)-2-oxopyrrolidin-3-yl)propan-2-yl)amino)-3-phenylpropan-2-yl)imidazo[1,2-a]pyridine-2-carboxamide (18i). 1H NMR (600 MHz, acetone- d_6): δ 9.40 (s, 1H), 8.79 (s, 1H), 8.53 (d, $J = 6.2$ Hz, 1H), 8.27 (d, $J = 4.9$ Hz, 1H), 8.04 (d, $J = 7.3$ Hz, 1H), 7.58–7.52 (m, 1H), 7.47–7.40 (m, 1H), 7.32 (t, $J = 6.4$ Hz, 2H), 7.28–7.22 (m, 2H), 7.18 (t, $J = 7.2$ Hz, 1H), 6.91 (s, 1H), 5.03–4.93 (m, 1H), 4.44 (m, 1H), 3.32 (t, $J = 6.9$ Hz, 1H), 3.27–3.23 (m, 1H), 2.45–2.26 (m, 2H), 1.99–1.94 (m, 1H), 1.80–1.75 (m, 1H), 1.37 (s, 1H), 1.29 (d, $J = 3.3$ Hz, 2H). ^{13}C NMR (150 MHz, acetone- d_6): δ 200.0, 178.9, 171.4, 161.5, 142.8, 137.3, 129.5, 129.3, 128.3, 128.2, 127.6, 126.6, 118.7, 114.8, 107.2, 98.7, 57.6, 54.0, 39.9, 38.4, 37.8, 30.8. HRMS (ESI) m/z : $[M + H]^+$ calcd for $C_{24}H_{25}BrN_5O_4$, 526.1084; found, 526.1093. Purity: 98.8%.

N-((S)-1-Oxo-1-(((S)-1-oxo-3-((S)-2-oxopyrrolidin-3-yl)propan-2-yl)amino)-3-phenylpropan-2-yl)benzofuran-2-carboxamide (18j). 1H NMR (500 MHz, acetone- d_6): δ 9.43 (s, 1H), 8.64 (d, $J = 6.8$ Hz, 1H), 8.11 (d, $J = 8.0$ Hz, 1H), 7.71 (d, $J = 7.5$ Hz, 1H), 7.56–7.50 (m, 1H), 7.49–7.41 (m, 2H), 7.37 (dd, $J = 9.2, 2.3$ Hz, 2H), 7.32–7.22 (m, 3H), 7.19 (d, $J = 7.5$ Hz, 1H), 7.12 (s, 1H), 5.10–5.01 (m, 1H), 4.58–4.32 (m, 1H), 3.38 (m, 1H), 3.25 (dd, $J = 9.0, 2.5$ Hz, 3H), 2.53–2.27 (m, 2H), 2.04 (m, 1H), 1.86–1.62 (m, 2H). ^{13}C NMR (125 MHz, acetone- d_6): δ 199.6, 178.8, 171.1, 157.8, 154.3, 148.5, 137.0, 129.0, 127.9, 127.1, 126.4, 126.1, 123.2, 122.2, 111.3, 109.6, 97.9, 57.1, 54.0, 39.6, 37.4. HRMS (ESI) m/z : $[M - H]^-$ calcd for $C_{25}H_{24}N_3O_5$, 446.1721; found, 446.172. Purity: 95.6%.

N-((S)-1-Oxo-1-(((S)-1-oxo-3-((S)-2-oxopyrrolidin-3-yl)propan-2-yl)amino)-3-phenylpropan-2-yl)quinoxaline-2-carboxamide (18k). 1H NMR (500 MHz, acetone- d_6): δ 9.47 (s, 1H), 8.69 (d, $J = 8.0$ Hz, 1H), 8.15 (m, 2H), 7.95 (m, 2H), 7.80 (d, $J = 8.0$ Hz, 1H), 7.34 (d, $J = 7.3$ Hz, 2H), 7.25 (t, $J = 7.3$ Hz, 2H), 7.18 (t, $J = 7.3$ Hz, 1H), 6.83 (s, 1H), 5.03–4.95 (m, 1H), 3.99 (dd, $J = 7.3, 4.3$ Hz, 1H), 3.50 (m, 2H), 3.31–3.20 (m, 3H), 2.39–2.28 (m, 2H), 1.95–1.87 (m, 1H), 1.78–1.68 (m, 1H), 1.62–1.51 (m, 1H). ^{13}C NMR (151 MHz, acetone- d_6): δ 199.5, 179.0, 170.7, 162.3, 143.1, 139.7, 136.7, 131.3, 130.6, 129.2, 129.1, 128.9, 127.9, 127.7, 126.2, 97.9, 57.4, 53.9, 53.6, 39.5, 37.6. HRMS (ESI) m/z : $[M - H]^-$ calcd for $C_{25}H_{24}N_5O_4$, 458.1834; found, 458.1823. Purity: 98.3%.

3-Methyl-N-((S)-1-oxo-1-(((S)-1-oxo-3-((S)-2-oxopyrrolidin-3-yl)propan-2-yl)amino)-3-phenylpropan-2-yl)quinoxaline-2-carboxamide (18l). 1H NMR (500 MHz, $CDCl_3$): δ 9.30 (s, 1H), 8.63 (d, $J = 8.5$ Hz, 1H), 8.33 (d, $J = 6.2$ Hz, 1H), 8.06 (d, $J = 7.5$ Hz, 1H), 8.02 (d, $J = 8.5$ Hz, 1H), 7.80 (m, 1H), 7.75 (dd, $J = 11.0, 4.0$ Hz, 1H), 7.39–7.27 (m, 5H), 7.25 (d, $J = 7.1$ Hz, 1H), 6.56 (s, 1H), 5.12 (q, $J = 7.1$ Hz, 1H), 4.32 (m, 1H), 3.31 (dd, $J = 12.8, 6.2$ Hz, 3H), 3.02 (s, 3H), 2.40–2.30 (m, 2H), 1.99–1.93 (m, 1H), 1.88–1.75 (m, 2H). ^{13}C NMR (125 MHz, $CDCl_3$): δ 199.8, 179.9, 171.8, 164.5, 153.9, 142.9, 139.1, 136.4, 131.7, 129.7, 129.6, 129.4, 128.6, 128.4, 127.1, 57.7, 54.5, 40.5, 39.1, 37.9, 29.7, 28.4, 24.5. HRMS (ESI) m/z : $[M + H]^+$ calcd for $C_{26}H_{28}N_5O_4$, 474.2136; found, 474.215. Purity: 98.8%.

N-((S)-1-Oxo-1-(((S)-1-oxo-3-((S)-2-oxopyrrolidin-3-yl)propan-2-yl)amino)-3-phenylpropan-2-yl)quinoline-2-carboxamide (18m). 1H NMR (500 MHz, $CDCl_3$): δ 9.22 (s, 1H), 8.84 (d, $J = 8.5$ Hz, 1H), 8.28 (d, $J = 8.5$ Hz, 1H), 8.22 (dd, $J = 10.1, 6.0$ Hz, 1H), 8.11 (m, 2H), 7.86 (d, $J = 8.1$ Hz, 1H), 7.77 (dd, $J = 11.2, 4.1$ Hz, 1H), 7.62 (m, 1H), 7.36–7.27 (m, 4H), 7.24 (t, $J = 7.2$ Hz, 1H), 5.08 (m, 1H), 4.33–4.28 (m, 1H), 3.35–3.29 (m, 2H), 3.25 (t, $J = 6.8$ Hz, 2H), 2.38–2.30 (m, 2H), 1.93–1.84 (m, 2H), 1.79–1.71 (m, 2H). ^{13}C NMR (125 MHz, $CDCl_3$): δ 199.8, 179.8, 171.7, 164.4, 149.1, 146.6, 137.4, 136.5, 129.6, 129.4, 128.6, 127.1, 118.7, 57.7, 54.7, 40.5, 39.0, 37.8, 29.6, 28.6. HRMS (ESI) m/z : $[M - H]^-$ calcd for $C_{26}H_{25}N_4O_4$, 457.1881; found, 457.1888. Purity: 95.2%.

7-Bromo-N-((S)-1-oxo-1-(((S)-1-oxo-3-((S)-2-oxopyrrolidin-3-yl)propan-2-yl)amino)-3-phenylpropan-2-yl)quinoline-2-carboxamide (18n). 1H NMR (600 MHz, acetone- d_6): δ 11.14 (d, $J = 8.4$ Hz, 1H), 9.41 (s, 1H), 8.28–8.23 (m, 1H), 7.78 (dd, $J = 12.5, 8.8$ Hz, 1H), 7.58 (d, $J = 1.8$ Hz, 1H), 7.47 (d, $J = 8.8$ Hz, 1H), 7.37–7.33 (m, 2H), 7.23 (d, $J = 7.7$ Hz, 2H), 7.16 (dd, $J = 6.3, 1.9$ Hz, 4H), 5.44 (m,

1H), 5.06 (dd, $J = 7.1, 4.5$ Hz, 1H), 4.51 (m, 1H), 4.13–3.99 (m, 1H), 3.32 (d, $J = 2.0$ Hz, 1H), 3.20 (m, 2H), 2.44–2.34 (m, 1H), 2.33–2.25 (m, 1H), 1.79–1.55 (m, 2H). ^{13}C NMR (150 MHz, acetone- d_6): δ 200.0, 178.9, 171.3, 163.3, 150.7, 147.0, 138.0, 137.2, 131.6, 131.3, 129.8, 129.7, 129.6, 128.4, 128.1, 126.7, 123.8, 119.1, 57.8, 54.6, 54.1, 39.9, 38.3, 37.9. HRMS (ESI) m/z : $[\text{M} - \text{H}]^-$ calcd for $\text{C}_{26}\text{H}_{24}\text{BrN}_4\text{O}_4$, 535.0986; found, 535.0992. Purity: 95.0%.

6-Chloro-*N*-((*S*)-1-oxo-1-((*S*)-1-oxo-3-((*S*)-2-oxopyrrolidin-3-yl)propan-2-yl)amino)-3-phenylpropan-2-yl)-2H-chromene-3-carboxamide (18o). ^1H NMR (600 MHz, CDCl_3): δ 9.24 (s, 1H), 8.55 (d, $J = 6.0$ Hz, 1H), 7.29–7.26 (m, 2H), 7.22 (m, 5H), 7.10 (m, 1H), 6.99 (d, $J = 2.6$ Hz, 1H), 6.95 (s, 1H), 6.72 (d, $J = 8.6$ Hz, 1H), 6.58 (s, 1H), 5.01 (dd, $J = 14.9, 6.9$ Hz, 1H), 4.91–4.85 (m, 2H), 4.25–4.20 (m, 1H), 3.32–3.26 (m, 2H), 3.18 (m, 2H), 2.34–2.29 (m, 2H), 1.94–1.87 (m, 1H), 1.82–1.77 (m, 1H). ^{13}C NMR (150 MHz, CDCl_3): δ 201.6, 181.9, 174.3, 166.5, 155.1, 138.2, 132.7, 131.4, 130.5, 129.6, 129.1, 129.0, 128.9, 128.3, 124.2, 119.2, 66.8, 59.9, 56.1, 42.6, 40.6, 40.1, 31.4, 30.5. HRMS (ESI) m/z : $[\text{M} - \text{H}]^-$ calcd for $\text{C}_{26}\text{H}_{25}\text{ClN}_3\text{O}_5$, 494.1488; found, 494.1481. Purity: 96.2%.

***N*-((*S*)-1-Oxo-1-((*S*)-1-oxo-3-((*S*)-2-oxopyrrolidin-3-yl)propan-2-yl)amino)-3-phenylpropan-2-yl)-1H-indole-2-carboxamide (18p).** ^1H NMR (600 MHz, acetone- d_6): δ 10.52 (s, 1H), 9.40 (s, 1H), 8.16 (d, $J = 13.6$ Hz, 1H), 7.73–7.62 (m, 2H), 7.45–7.40 (m, 1H), 7.39 (d, $J = 2.4$ Hz, 1H), 7.35 (t, $J = 7.6$ Hz, 2H), 7.28–7.21 (m, 2H), 7.18 (t, $J = 6.6$ Hz, 1H), 6.94–6.78 (m, 1H), 6.54 (s, 1H), 5.45–4.98 (m, 1H), 4.97–4.39 (m, 1H), 4.34–3.82 (m, 1H), 3.26–3.16 (m, 3H), 2.45–2.22 (m, 2H), 2.00–1.86 (m, 1H), 1.81–1.43 (m, 2H). ^{13}C NMR (125 MHz, acetone- d_6): δ 200.0, 179.6, 172.1, 161.6, 137.6, 137.0, 131.0, 129.5, 129.4, 128.3, 128.2, 127.7, 126.5, 123.9, 121.7, 120.0, 112.3, 103.5, 57.6, 54.9, 40.1, 37.9, 37.8. HRMS (ESI) m/z : $[\text{M} - \text{H}]^-$ calcd for $\text{C}_{25}\text{H}_{25}\text{N}_4\text{O}_4$, 445.1881; found, 445.1881. Purity: 97.0%.

5-Methyl-*N*-((*S*)-3-methyl-1-oxo-1-((*S*)-1-oxo-1-((*S*)-1-oxo-3-((*S*)-2-oxopyrrolidin-3-yl)propan-2-yl)amino)-3-phenylpropan-2-yl)amino)butan-2-yl)isoxazole-3-carboxamide (26a). ^1H NMR (500 MHz, acetone- d_6): δ 9.35 (s, 1H), 8.30 (d, $J = 6.8$ Hz, 1H), 7.81–7.69 (m, 1H), 7.58 (d, $J = 8.4$ Hz, 1H), 7.31–7.22 (m, 4H), 7.17 (t, $J = 7.1$ Hz, 1H), 6.94 (s, 1H), 6.52 (d, $J = 0.7$ Hz, 1H), 4.79 (m, 1H), 4.54–4.43 (m, 1H), 4.27 (m, 1H), 3.32–3.18 (m, 3H), 3.04 (dd, $J = 13.8, 8.1$ Hz, 1H), 2.44–2.28 (m, 2H), 2.22 (dd, $J = 13.4, 6.7$ Hz, 1H), 1.93 (d, $J = 5.6$ Hz, 1H), 1.81–1.72 (m, 2H), 1.31 (s, 2H), 0.93 (dd, $J = 10.3, 6.8$ Hz, 6H). ^{13}C NMR (125 MHz, acetone- d_6): δ 199.4, 178.5, 171.1, 171.0, 169.8, 158.2, 136.9, 128.9, 127.7, 126.0, 100.7, 57.7, 56.9, 54.2, 39.4, 37.23, 37.2, 29.1, 27.7, 18.3, 16.9, 10.7. HRMS (ESI) m/z : $[\text{M} - \text{H}]^-$ calcd for $\text{C}_{26}\text{H}_{33}\text{N}_5\text{O}_6$, 510.2358; found, 510.2352. Purity: 96.7%.

***N*-((*S*)-3-Methyl-1-oxo-1-((*S*)-1-oxo-1-((*S*)-1-oxo-3-((*S*)-2-oxopyrrolidin-3-yl)propan-2-yl)amino)-3-phenylpropan-2-yl)amino)butan-2-yl)-1H-indole-2-carboxamide (26b).** ^1H NMR (500 MHz, acetone- d_6): δ 11.20 (s, 1H), 9.46 (s, 1H), 8.22 (d, $J = 7.4$ Hz, 1H), 7.96–7.88 (m, 1H), 7.75 (dd, $J = 11.9, 4.0$ Hz, 1H), 7.62 (m, 2H), 7.33–7.29 (m, 1H), 7.26–7.20 (m, 3H), 7.19–7.06 (m, 4H), 7.03 (dd, $J = 16.8, 9.5$ Hz, 1H), 4.88–4.80 (m, 1H), 4.54–4.32 (m, 2H), 3.38 (dd, $J = 19.0, 10.1$ Hz, 1H), 3.32–3.24 (m, 2H), 3.00 (m, 1H), 2.43 (m, 1H), 2.32 (m, 2H), 2.23 (tt, $J = 9.0, 4.5$ Hz, 1H), 1.87–1.81 (m, 1H), 1.31 (d, $J = 1.7$ Hz, 1H), 0.96 (dd, $J = 10.7, 6.9$ Hz, 6H). ^{13}C NMR (125 MHz, acetone- d_6): δ 199.8, 179.2, 171.5, 170.2, 162.5, 137.2, 130.2, 128.6, 127.7, 125.8, 123.4, 121.1, 119.6, 112.2, 103.2, 60.0, 56.7, 54.2, 39.5, 37.3, 36.5, 30.3, 29.5, 29.1, 27.0, 18.1, 17.5. HRMS (ESI) m/z : $[\text{M} - \text{H}]^-$ calcd for $\text{C}_{30}\text{H}_{34}\text{N}_5\text{O}_5$, 544.2565; found, 544.2568. Purity: 97.6%.

***N*-((*S*)-3-Methyl-1-oxo-1-((*S*)-1-oxo-1-((*S*)-1-oxo-3-((*S*)-2-oxopyrrolidin-3-yl)propan-2-yl)amino)-3-phenylpropan-2-yl)amino)butan-2-yl)benzofuran-2-carboxamide (26c).** ^1H NMR (500 MHz, acetone- d_6): δ 9.37 (s, 1H), 8.36 (d, $J = 7.1$ Hz, 1H), 8.02 (d, $J = 8.1$ Hz, 1H), 7.77 (d, $J = 7.8$ Hz, 1H), 7.60 (t, $J = 6.2$ Hz, 2H), 7.48 (dd, $J = 8.4, 7.5$ Hz, 1H), 7.34 (t, $J = 7.5$ Hz, 1H), 7.30–7.26 (m, 2H), 7.21–7.03 (m, 4H), 4.86 (m, 1H), 4.63–4.55 (m, 1H), 4.51–4.30 (m, 1H), 4.07 (d, $J = 2.6$ Hz, 1H), 3.30–3.16 (m, 3H), 3.05 (dd, $J = 13.9, 8.2$ Hz, 1H), 2.43–2.18 (m, 3H), 2.05–1.97 (m, 1H), 1.84–1.75 (m, 1H), 1.60 (m, 1H), 0.98 (dd, $J = 6.6, 2.2$ Hz, 6H). ^{13}C NMR (125 MHz, acetone- d_6): δ 199.5, 179.5, 178.8, 171.2, 170.2, 158.0, 154.3, 148.5, 136.9, 128.9, 127.7, 126.5, 125.9, 123.2, 122.2, 111.3, 109.8, 58.0, 56.8, 54.3, 53.6,

39.5, 37.3, 30.5, 18.4, 17.4. HRMS (ESI) m/z : $[\text{M} - \text{H}]^-$ calcd for $\text{C}_{30}\text{H}_{33}\text{N}_4\text{O}_6$, 545.2406; found, 545.2407. Purity: 98.7%.

***N*-((*S*)-3-Methyl-1-oxo-1-((*S*)-1-oxo-1-((*S*)-1-oxo-3-((*S*)-2-oxopyrrolidin-3-yl)propan-2-yl)amino)-3-phenylpropan-2-yl)amino)butan-2-yl)quinoline-2-carboxamide (26d).** ^1H NMR (500 MHz, acetone- d_6): δ 9.40 (s, 1H), 8.74 (d, $J = 8.5$ Hz, 1H), 8.52 (d, $J = 8.5$ Hz, 1H), 8.27 (d, $J = 8.5$ Hz, 1H), 8.14 (d, $J = 8.5$ Hz, 1H), 8.06 (d, $J = 8.0$ Hz, 1H), 7.96 (d, $J = 8.0$ Hz, 1H), 7.88–7.82 (m, 1H), 7.72 (dd, $J = 11.2, 4.0$ Hz, 1H), 7.29 (d, $J = 7.4$ Hz, 2H), 7.19 (t, $J = 7.6$ Hz, 2H), 7.09 (d, $J = 7.5$ Hz, 1H), 4.85 (dd, $J = 11.2, 5.0$ Hz, 1H), 4.62–4.55 (m, 1H), 4.40–4.30 (m, 1H), 3.33–3.20 (m, 3H), 3.06–3.00 (m, 1H), 2.50–2.41 (m, 1H), 2.38–2.27 (m, 2H), 2.06–2.00 (m, 1H), 1.80 (t, $J = 12.9, 9.6$ Hz, 2H), 1.30 (d, $J = 5.1$ Hz, 1H), 0.99 (dd, $J = 19.0, 6.8$ Hz, 6H). ^{13}C NMR (125 MHz, acetone- d_6): δ 199.5, 178.7, 171.2, 170.3, 163.7, 149.2, 145.9, 137.4, 137.0, 129.9, 129.1, 128.8, 127.7, 127.6, 127.5, 125.9, 118.2, 58.0, 56.8, 54.3, 39.5, 37.3, 37.2, 30.8, 18.5, 17.0. HRMS (ESI) m/z : $[\text{M} - \text{H}]^-$ calcd for $\text{C}_{31}\text{H}_{35}\text{N}_5\text{O}_5$, 556.2565; found, 556.2562. Purity: 95.4%.

***N*-((*S*)-3-Methyl-1-oxo-1-((*S*)-1-oxo-1-((*S*)-1-oxo-3-((*S*)-2-oxopyrrolidin-3-yl)propan-2-yl)amino)-3-phenylpropan-2-yl)amino)butan-2-yl)-2,3-dihydrobenzo[b][1,4]dioxine-6-carboxamide (26e).** ^1H NMR (500 MHz, acetone- d_6): δ 9.35 (s, 1H), 8.32 (d, $J = 7.1$ Hz, 1H), 7.88 (d, $J = 8.1$ Hz, 1H), 7.61 (s, 1H), 7.46 (dd, $J = 6.5, 2.1$ Hz, 2H), 7.26 (d, $J = 7.1$ Hz, 2H), 7.20 (t, $J = 7.4$ Hz, 2H), 7.14 (s, 1H), 6.89 (d, $J = 9.0$ Hz, 1H), 4.81 (m, 1H), 4.45 (dd, $J = 15.3, 7.4$ Hz, 1H), 4.36–4.27 (m, 5H), 3.30–3.23 (m, 2H), 3.18–3.03 (m, 2H), 2.44–2.28 (m, 2H), 2.21 (d, $J = 7.0$ Hz, 1H), 1.98–1.92 (m, 1H), 1.77 (dd, $J = 9.0, 3.1$ Hz, 2H), 1.31 (s, 1H), 0.95 (t, $J = 7.3$ Hz, 6H). ^{13}C NMR (125 MHz, acetone- d_6): δ 199.5, 171.2, 170.8, 165.9, 146.2, 142.8, 136.9, 128.9, 127.7, 127.0, 125.9, 120.4, 116.3, 64.1, 63.7, 59.0, 54.1, 37.3, 37.2, 29.2, 18.5, 17.6. HRMS (ESI) m/z : $[\text{M} - \text{H}]^-$ calcd for $\text{C}_{30}\text{H}_{35}\text{N}_4\text{O}_7$, 563.2511; found, 563.2501. Purity: 95.1%.

Materials and Methods. Protein Expression and Purification. The full-length gene encoding the EV71 3C^{pro} and the SARS-CoV-2 3CL^{pro} with an *N*-terminal 6 × His-SUMO2 fusion tag was cloned into the pET-15b vector. The resulting plasmids were transformed into BL21 (DE3) cells for protein expression. The expressed proteins were purified by a Ni-NTA column (GE) and transformed into the cleavage buffer (25 mM Tris, pH 7.5, 300 mM NaCl, 2 mM DTT) containing SUMO Specific Peptidase 2 (SEN2P) for removing the 6 × His-SUMO2 fusion tag. The resulting protein samples were further purified by Q-Sepharose (GE Healthcare) and Superdex200 (GE Healthcare). The eluted EV71 3C^{pro} and SARS-CoV-2 3CL^{pro} were stored in a solution containing 25 mM Tris (pH 8.0), 500 mM NaCl, and 2 mM DTT, and in a solution containing 10 mM Tris (pH 7.5), respectively.

Protein Crystallization and Structure Determination. The purified EV71 3C^{pro} was concentrated to 10 mg/mL and incubated 1 h with 2 mM 18p before crystallization condition screening. Crystallization was performed at 20 °C using a hanging drop vapor-diffusion method, by mixing equal volumes (1:1 μL) of the protein and crystallization solution. Crystals were finally yielded in a solution containing 0.1 M MES monohydrate (pH 6.0), 20% 2-propanol, and 20% polyethylene glycol monomethyl ether 2000. Then, crystals were flash-frozen in liquid nitrogen in the presence of the reservoir solution supplemented with 20% glycerol. X-ray diffraction data were collected at beamline BL18U1 at the Shanghai Synchrotron Radiation Facility.¹³ The data were processed with HKL3000 software packages.¹⁴ The complex structure was solved by molecular replacement using the program PHASER¹⁵ with a search model of PDB code 4GHT. The model was built using Coot¹⁶ and refined with a simulated-annealing protocol implemented in the program PHENIX.¹⁷ The refined structure was deposited to the Protein Data Bank with an accession code, 7DNC.

Inhibition Assays of the EV71 3C^{pro} and the SARS-CoV-2 3CL^{pro}. A fluorescence resonance energy transfer (FRET) protease assay was applied to measure the inhibitory activity of compounds against the EV71 3C^{pro}. The fluorogenic substrate Dacyl-KTSAVLQSGFRKME-Edans was synthesized by GenScript (Nanjing, China). The assay was performed in a total volume of 120 μL . The recombinant EV71 3C^{pro} at a final concentration of 5 μM was mixed with serial dilutions of each compound in 80 μL of assay buffer (25 mM Tris, pH 8.0, 150 mM

NaCl, and 10% glycerol) and incubated for 10 min. The reaction was initiated by adding 40 μL of a fluorogenic substrate at a final concentration of 25 μM . The reaction solution was then incubated at 30 $^{\circ}\text{C}$ for 3 h. After that, the fluorescence signal at 340 nm (excitation)/490 nm (emission) was measured immediately with a Bio-Tek Synergy4 plate reader.

The inhibition assay of the SARS-CoV-2 3CL^{pro} has been described previously.¹⁸ In brief, the recombinant SARS-CoV-2 3CL^{pro} at a concentration of 30 nM was mixed with serial dilutions of each compound in 80 μL of assay buffer (50 mM Tris–HCl, pH 7.3, 1 mM EDTA) and incubated for 10 min. The reaction was initiated by adding 40 μL of a fluorogenic substrate (MCA-AVLQSGFR-Lys(Dnp)-Lys-NH₂) at a final concentration of 20 μM . After that, the fluorescence signal at 320 nm (excitation)/405 nm (emission) was measured immediately every 35 s for 3.5 min with a Bio-Tek Synergy4 plate reader. The velocities of reactions with compounds added at various concentrations compared to the reaction added with DMSO were calculated and used to generate inhibition profiles. For each compound, at least three independent experiments were performed for the determination of IC₅₀ values. The IC₅₀ values were expressed as the mean \pm SD and determined via nonlinear regression analysis using GraphPad Prism software 8.0 (GraphPad Software, Inc., San Diego, CA, USA).

Cells. RD cells were maintained in MEM Rega-3 medium supplemented with 2% FBS, 2 mM L-glutamine, and 0.075% NaHCO₃, all supplied by Gibco, Life Technologies. Cells were maintained at 37 $^{\circ}\text{C}$ in a humidified atmosphere of 5% CO₂.

The Vero E6 cell line was obtained from American Type Culture Collection (ATCC, no. 1586) and maintained in Dulbecco's modified Eagle medium (DMEM; Gibco Invitrogen) supplemented with 10% fetal bovine serum (FBS; Gibco Invitrogen), 1% antibiotic/antimycotic (Gibco Invitrogen), at 37 $^{\circ}\text{C}$ in a humidified 5% CO₂ incubator.

Viruses. Enterovirus 71 strain BrCr (EV71 BrCr), kindly provided by Prof. Dr. F. van Kuppeveld (Universiteit Utrecht, The Netherlands), was grown on RD cells. When a full cytopathic effect (CPE) was observed, the virus was harvested from the supernatants after centrifugation (10 min, 3000 rpm) and stored at -80°C . The viral titer was determined by end point titration.

A clinical isolate of SARS-CoV-2 (nCoV-2019BetaCoV/Wuhan/WIV04/2019) was propagated in Vero E6 cells, and a viral titer was determined by TCID₅₀.^{8a} All infection experiments were performed at biosafety level-3 (BSL-3).

Antiviral Assay. The anti-EV71 activity of selected compounds was tested in RD cells and seeded in a 96-well plate (2.5 \times 10⁴ cells/well). Cells were allowed to adhere overnight, after which cells were infected with EV71; a serial dilution of selected compounds was added and incubated for 4 days, i.e., until complete CPE was observed in the untreated and infected virus control conditions. CPE was subsequently quantified using an MTS-reduction assay (MTS = 3-(4,5-dimethylthiazol-2-yl)-5-(3-carboxymethoxyphenyl)-2-(4-sulfophenyl)-2H-tetrazolium, inner salt). For this, a MTS/phenazine methosulfate (PMS) stock solution (2 mg/mL MTS (Promega, Leiden, The Netherlands) and 46 $\mu\text{g}/\text{mL}$ PMS (Sigma-Aldrich, Bornem, Belgium) in PBS at pH 6–6.5) was diluted 1:20 in MEM (Life Technologies, Gent, Belgium cat. no. 21090-022). The medium was aspirated from wells, and 75 μL of MTS/PMS solution was added. After 1–2 h of incubation at 37 $^{\circ}\text{C}$, the absorbance was measured at 498 nm. The % inhibition for each well is then calculated by normalization of the absorbance to the condition of untreated-infected cells (=0% inhibition) and the condition of untreated-uninfected cells (=100% inhibition). From the obtained dose–response curve, the EC₅₀ is calculated by curve fitting using Dotmatics software.

To assess the antiviral activity of compounds against SARS-CoV-2, preseeded Vero E6 cells (5 \times 10⁴ cells/well) were treated with different concentrations of the indicated compounds for 1 h and then were infected with SARS-CoV-2 at an MOI of 0.01. At 24 h pi, the cell supernatant was collected, and a viral RNA copy number in the cell supernatant was measured using real-time PCR, as described previously.¹⁹

The antiviral activity of selected compounds against EV68, CoxA21, CoxB3, RV-A02, and RV-B14 was tested as described previously.²⁰

To assess the cytotoxicity of the test compounds, Vero E6 cells preseeded in a 96-well dish (2 \times 10⁴ cells/well) were treated with different concentrations of the indicated compounds, and 24 h later, the relative numbers of surviving cells were measured with cell counting kit-8 (GK10001, GLPBIO) according to the manufacturer's instructions.

Pharmacokinetic Profiles in CD-1 Mice. Male CD-1 mice ($n = 3$ per group) were treated with a solution of compounds **18p** and **26d** (DMSO/EtOH/PEG300/NaCl (5:5:40:50, v/v/v/v)) at doses of 20 mg/kg, 5 mg/kg, and 5 mg/kg via intraperitoneal (ip), subcutaneous (sc), and intravenous (iv), respectively. Blood samples were collected at 0.05, 0.25, 0.75, 2, 4, 8, and 24 h after administration. Serum samples were obtained through common procedures, and the concentrations of the compound in the supernatant were analyzed by LC-MS/MS.

All procedures relating to animal handling, care, and treatment were performed according to the guidelines approved by the Institutional Animal Care and Use Committee of the contract research organizations performing the study.

■ ASSOCIATED CONTENT

Supporting Information

The Supporting Information is available free of charge at <https://pubs.acs.org/doi/10.1021/acs.jmedchem.0c02258>.

An overlay of EV71 3C^{pro}-**18p** and **AG7088** complex structures; the binding pocket of 3C^{pro} of CoXB3, RV-A02, and EV71; the anti-SARS-CoV-2 activities of compounds; the ¹H NMR and ¹³C NMR spectra of target compounds; the purity of target compounds; and the crystallography data collection and refinement statistics (PDF)

Molecular formula stings (CSV)

Accession Codes

The atomic coordinates and structure factors have been deposited into the Protein Data Bank with accession code 7DNC (EV71 3C^{pro}-**18p**). The authors will release the atomic coordinates and experimental data upon article publication.

■ AUTHOR INFORMATION

Corresponding Authors

Leike Zhang – State Key Laboratory of Virology, Wuhan Institute of Virology, Center for Biosafety Mega-Science, Chinese Academy of Sciences, Wuhan, Hubei 430071, China; orcid.org/0000-0002-2593-2571; Email: zhangleike@wh.iov.cn

Yechun Xu – State Key Laboratory of Drug Research, CAS Key Laboratory of Receptor Research, Shanghai Institute of Materia Medica, Chinese Academy of Sciences, Shanghai 201203, China; University of Chinese Academy of Sciences, School of Pharmaceutical Science and Technology, Hangzhou Institute for Advanced Study, Beijing 100049, China; orcid.org/0000-0002-1581-6155; Email: yxcu@simm.ac.cn

Johan Neyts – KU Leuven, Department of Microbiology and Immunology, Rega Institute for Medical Research, Laboratory of Virology and Chemotherapy, Leuven B-3000, Belgium; Email: johan.neyts@kuleuven.be

Hong Liu – State Key Laboratory of Drug Research, CAS Key Laboratory of Receptor Research, Shanghai Institute of Materia Medica, Chinese Academy of Sciences, Shanghai 201203, China; College of Pharmacy, Nanjing University of Chinese Medicine, Nanjing 210023, China; University of Chinese Academy of Sciences, School of Pharmaceutical Science and Technology, Hangzhou Institute for Advanced Study,

Beijing 100049, China; orcid.org/0000-0003-3685-6268;
Email: hliu@simmm.ac.cn

Materia Medica, Chinese Academy of Sciences, Shanghai
201203, China; University of Chinese Academy of Sciences,
Beijing 100049, China

Authors

- Wenhao Dai** – State Key Laboratory of Drug Research, CAS Key Laboratory of Receptor Research, Shanghai Institute of Materia Medica, Chinese Academy of Sciences, Shanghai 201203, China; University of Chinese Academy of Sciences, Beijing 100049, China
- Dirk Jochmans** – KU Leuven, Department of Microbiology and Immunology, Rega Institute for Medical Research, Laboratory of Virology and Chemotherapy, Leuven B-3000, Belgium
- Hang Xie** – State Key Laboratory of Drug Research, CAS Key Laboratory of Receptor Research, Shanghai Institute of Materia Medica, Chinese Academy of Sciences, Shanghai 201203, China
- Hang Yang** – State Key Laboratory of Virology, Wuhan Institute of Virology, Center for Biosafety Mega-Science, Chinese Academy of Sciences, Wuhan, Hubei 430071, China
- Jian Li** – State Key Laboratory of Drug Research, CAS Key Laboratory of Receptor Research, Shanghai Institute of Materia Medica, Chinese Academy of Sciences, Shanghai 201203, China; College of Pharmacy, Nanjing University of Chinese Medicine, Nanjing 210023, China
- Haixia Su** – State Key Laboratory of Drug Research, CAS Key Laboratory of Receptor Research, Shanghai Institute of Materia Medica, Chinese Academy of Sciences, Shanghai 201203, China; University of Chinese Academy of Sciences, Beijing 100049, China
- Di Chang** – Shanghai Key Laboratory of New Drug Design, School of Pharmacy, East China University of Science and Technology, Shanghai 200237, China
- Jiang Wang** – State Key Laboratory of Drug Research, CAS Key Laboratory of Receptor Research, Shanghai Institute of Materia Medica, Chinese Academy of Sciences, Shanghai 201203, China; University of Chinese Academy of Sciences, School of Pharmaceutical Science and Technology, Hangzhou Institute for Advanced Study, Beijing 100049, China
- Jingjing Peng** – State Key Laboratory of Drug Research, CAS Key Laboratory of Receptor Research, Shanghai Institute of Materia Medica, Chinese Academy of Sciences, Shanghai 201203, China; University of Chinese Academy of Sciences, Beijing 100049, China
- Lili Zhu** – Shanghai Key Laboratory of New Drug Design, School of Pharmacy, East China University of Science and Technology, Shanghai 200237, China
- Yong Nian** – State Key Laboratory of Drug Research, CAS Key Laboratory of Receptor Research, Shanghai Institute of Materia Medica, Chinese Academy of Sciences, Shanghai 201203, China; College of Pharmacy, Nanjing University of Chinese Medicine, Nanjing 210023, China
- Rolf Hilgenfeld** – Institute of Molecular Medicine and German Center for Infection Research (DZIF), University of Lübeck, 23562 Lübeck, Germany; orcid.org/0000-0001-8850-2977
- Hualiang Jiang** – State Key Laboratory of Drug Research, CAS Key Laboratory of Receptor Research, Shanghai Institute of Materia Medica, Chinese Academy of Sciences, Shanghai 201203, China; University of Chinese Academy of Sciences, School of Pharmaceutical Science and Technology, Hangzhou Institute for Advanced Study, Beijing 100049, China
- Kaixian Chen** – State Key Laboratory of Drug Research, CAS Key Laboratory of Receptor Research, Shanghai Institute of

Complete contact information is available at:

<https://pubs.acs.org/10.1021/acs.jmedchem.0c02258>

Author Contributions

[○]W.D., D.J., H.X., and H.Y. contributed equally to this work.

Notes

The authors declare no competing financial interest.

ACKNOWLEDGMENTS

We are grateful to the National Natural Science Foundation of China (21632008, 21672231, 21877122, 21877118, and 81620108027), the Strategic Priority Research Program of the Chinese Academy of Sciences (XDA12040107 and XDA12040201), and the Youth Innovation Promotion Association CAS (grants 2018367 to L.-K.Z.) for financial support

ABBREVIATIONS USED

EV71, enterovirus 71; HFMD, hand, foot, and mouth disease; SARS-CoV-2, severe acute respiratory syndrome coronavirus 2; COVID-19, coronavirus disease 2019; 3C^{pro}, 3C protease; 3CL^{pro}, 3C-like protease; HRV, human rhinoviruses; EV68, enterovirus 68; CoxA21, coxsackievirus A21; DMP, Dess–Martin periodinane; SAR, structure–activity relationship; PDB, protein data bank; HATU, *O*-(7-; 2-(7-azabenzotriazol-1-yl)-*N,N,N,N'*-tetramethyluronium hexafluorophosphate; DIPEA, *N,N*-diisopropyl-ethyl-amine; TLC, thin-layer chromatography; HRMS, high-resolution mass spectra

REFERENCES

- (1) (a) Schmidt, N. J.; Lennette, E. H.; Ho, H. H. An apparently new enterovirus isolated from patients with disease of the central nervous system. *J. Infect. Dis.* **1974**, *129*, 304–309. (b) Chen, C. Y.; Chang, Y. C.; Huang, C. C.; Lui, C. C.; Lee, K. W.; Huang, S. C. Acute flaccid paralysis in infants and young children with enterovirus 71 infection: MR imaging findings and clinical correlates. *Am. J. Neuroradiol.* **2001**, *22*, 200–205. (c) Yang, Y.; Wang, H.; Gong, E.; Du, J.; Zhao, X.; McNutt, M. A.; Wang, S.; Zhong, Y.; Gao, Z.; Zheng, J. Neuropathology in 2 cases of fatal enterovirus type 71 infection from a recent epidemic in the People's Republic of China: a histopathologic, immunohistochemical, and reverse transcription polymerase chain reaction study. *Hum. Pathol.* **2009**, *40*, 1288–1295. (d) McMinn, P. C. An overview of the evolution of enterovirus 71 and its clinical and public health significance. *FEMS Microbiol. Rev.* **2002**, *26*, 91–107. (e) Lin, J. Y.; Chen, T. C.; Weng, K. F.; Chang, S. C.; Chen, L. L.; Shih, S. R. Viral and host proteins involved in picornavirus life cycle. *J. Biomed. Sci.* **2009**, *16*, 103–117. (f) Lin, Y. W.; Wang, S. W.; Tung, Y. Y.; Chen, S. H. Enterovirus 71 infection of human dendritic cells. *Exp. Biol. Med.* **2009**, *234*, 1166–1173.
- (2) (a) Chou, A. H.; Liu, C. C.; Chang, C. P.; Guo, M. S.; Hsieh, S. Y.; Yang, W. H.; Chao, H. J.; Wu, C. L.; Huang, J. L.; Lee, M. S.; Hu, A. Y. C.; Lin, S. C.; Huang, Y. Y.; Hu, M. H.; Chow, Y. H.; Chiang, J. R.; Chang, J. Y.; Chong, P. Pilot scale production of highly efficacious and stable enterovirus 71 vaccine candidates. *PLoS One* **2012**, *7*, e34834. (b) Zhu, F. C.; Liang, Z. L.; Li, X. L.; Ge, H. M.; Meng, F. Y.; Mao, Q. Y.; Zhang, Y. T.; Hu, Y. M.; Zhang, Z. Y.; Li, J. X.; Gao, F.; Chen, Q. H.; Zhu, Q. Y.; Chu, K.; Wu, X.; Yao, X.; Guo, H. J.; Chen, X. Q.; Liu, P.; Dong, Y. Y.; Li, F. X.; Shen, X. L.; Wang, J. Z. Immunogenicity and safety of an enterovirus 71 vaccine in healthy Chinese children and infants: a randomised, double-blind, placebo-controlled phase 2 clinical trial. *Lancet* **2013**, *381*, 1037–1045.

(3) (a) Stanway, G. Structure, function and evolution of picornaviruses. *J. Gen. Virol.* **1990**, *71*, 2483–2501. (b) Binford, S. L.; Maldonado, F.; Brothers, M. A.; Weady, P. T.; Zalman, L. S.; Meador, J. W., III; Matthews, D. A.; Patick, A. K. Conservation of amino acids in human rhinovirus 3C protease correlates with broad-spectrum antiviral activity of Rupintrivir, a novel human rhinovirus 3C protease inhibitor. *Antimicrob. Agents Chemother.* **2005**, *49*, 619–626. (c) Matthews, D. A.; Smith, W. W.; Ferre, R. A.; Condon, B.; Budahazi, G.; Sllson, W.; Villafranca, J. E.; Janson, C. A.; McElroy, H. E.; Gribskov, C. L.; Worland, S. Structure of human rhinovirus 3C protease reveals a trypsin-like polypeptide fold, RNA-binding site, and means for cleaving precursor polyprotein. *Cell* **1994**, *77*, 761–771. (d) Shih, S. R.; Chiang, C.; Chen, T. C.; Wu, C. N.; Hsu, J. T. A.; Lee, J. C.; Hwang, M. J.; Li, M. L.; Chen, G. W.; Ho, M. S. Mutations at KFRDI and VGK domains of enterovirus 71 3C protease affect its RNA binding and proteolytic activities. *J. Biomed. Sci.* **2004**, *11*, 239–248. (e) Wu, Y.; Lou, Z.; Miao, Y.; Yu, Y.; Dong, H.; Peng, W.; Bartlam, M.; Li, X.; Rao, Z. Structures of EV71 RNA-dependent RNA polymerase in complex with substrate and analogue provide a drug target against the hand-foot-and-mouth disease pandemic in China. *Protein Cell* **2010**, *1*, 491–500. (f) Shang, L.; Xu, M.; Yin, Z. Antiviral drug discovery for the treatment of enterovirus 71 infections. *Antiviral Res.* **2013**, *97*, 183–194.

(4) (a) Weng, K. F.; Li, M. L.; Hung, C. T.; Shih, S. R. Enterovirus 71 3C protease cleaves a novel target Cstf-64 and inhibits cellular polyadenylation. *PLoS Pathog.* **2009**, *5*, e1000593. (b) Kim, Y.; Lovell, S.; Tiew, K. C.; Mandadapu, S. R.; Alliston, K. R.; Battaile, K. P.; Groutas, W. C.; Chang, K. O. Broad-spectrum antivirals against 3C or 3C-like proteases of picornaviruses, noroviruses, and coronaviruses. *J. Virol.* **2012**, *86*, 11754–11762. (c) Xiong, M.; Su, H.; Zhao, W.; Xie, H.; Shao, Q.; Xu, Y. What coronavirus 3C-like protease tells us: From structure, substrate selectivity, to inhibitor design. *Med. Res. Rev.* **2021**, *3*, 1–34.

(5) (a) Hayden, F. G.; Turner, R. B.; Gwaltney, J. M.; Chi-Burris, K.; Gersten, M.; Hsyu, P.; Patick, A. K.; Smith, G. J.; Zalman, L. S. Phase II, randomized, double-blind, placebo-controlled studies of Rupintrivir nasal spray 2-percent suspension for prevention and treatment of experimentally induced rhinovirus colds in healthy volunteers. *Antimicrob. Agents Chemother.* **2003**, *47*, 3907–3916. (b) Kuo, C. J.; Shie, J. J.; Fang, J. M.; Yen, G. R.; Hsu, J. T. A.; Liu, H. G.; Tseng, S. N.; Chang, S. C.; Lee, C. Y.; Shih, S. R.; Liang, P. H. Design, synthesis, and evaluation of 3C protease inhibitors as anti-enterovirus 71 agents. *Bioorg. Med. Chem.* **2008**, *16*, 7388–7398. (c) Zhai, Y.; Ma, Y.; Ma, F.; Nie, Q.; Ren, X.; Wang, Y.; Shang, L.; Yin, Z. Structure-activity relationship study of peptidomimetic aldehydes as enterovirus 71 3C protease inhibitors. *Eur. J. Med. Chem.* **2016**, *124*, 559–573. (d) Wang, Y.; Yang, B.; Zhai, Y.; Yin, Z.; Sun, Y.; Rao, Z. A peptidyl aldehyde NK-1.8k suppresses EV71 and EV68 infection by targeting at 3C^{pro}. *Antimicrob. Agents Chemother.* **2015**, *59*, 2636–2646. (e) Zhai, Y.; Zhao, X.; Cui, Z.; Wang, M.; Wang, Y.; Li, L.; Sun, Q.; Yang, X.; Zeng, D.; Liu, Y.; Sun, Y.; Lou, Z.; Shang, L.; Yin, Z. Cyanohydrin as an Anchoring Group for Potent and Selective Inhibitors of Enterovirus 71 3C Protease. *J. Med. Chem.* **2015**, *58*, 9414–9420. (f) Ma, Y.; Li, L.; He, S.; Shang, C.; Sun, Y.; Liu, N.; Meek, T. D.; Wang, Y.; Shang, L. Application of dually activated Michael acceptor to the rational design of reversible covalent inhibitor for enterovirus 71 3C protease. *J. Med. Chem.* **2019**, *62*, 6146–6162. (g) Zhang, L.; Lin, D.; Kusov, Y.; Nian, Y.; Ma, Q.; Wang, J.; Brunn, A von.; Leyssen, P.; Lanko, K.; Neyts, J.; Wilde, A. de.; Snijder, E. J.; Liu, H.; Hilgenfeld, R. α -Ketoamides as broad-spectrum inhibitors of coronavirus and enterovirus replication: structure-based design, synthesis, and activity assessment. *J. Med. Chem.* **2020**, *63*, 4562–4578. (h) Ma, Y.; Shang, C.; Yang, P.; Li, L.; Zhai, Y.; Yin, Z.; Wang, B.; Shang, L. 4-Iminooxazolidin-2-one as a bioisostere of the cyanohydrin moiety: Inhibitors of enterovirus 71 3C protease. *J. Med. Chem.* **2018**, *61*, 10333–10339. (i) Li, P.; Yang, B.; Hao, F.; Wang, P.; He, H.; Huang, L.; Zhang, X.; Zhang, S.; Peng, X.; Yin, K.; Hu, J.; Chen, X.; Gu, Z.; Wang, L.; Shen, L.; Hu, G.; Li, N.; Li, J.; Chen, S.; Xiao, W.; Wang, Z.; Guo, Q.; Chang, X.; Zhang, L.; Cai, Q.; Lin, T. Design, synthesis, and biological evaluation of anti-EV71 agents. *Bioorg. Med. Chem. Lett.* **2016**, *26*, 3346–3350. (j) Kim, Y.; Shivanna, V.;

Narayanan, S.; Prior, A. M.; Weerasekara, S.; Hua, D. H.; Kankanamalage, A. C. G.; Groutas, W. C.; Chang, K.-O. Broad-spectrum inhibitors against 3C-like proteases of feline coronaviruses and feline caliciviruses. *J. Virol.* **2015**, *89*, 4942–4950. (k) Prior, A. M.; Kim, Y.; Weerasekara, S.; Moroze, M.; Alliston, K. R.; Uy, R. A.; Groutas, W. C.; Chang, K. O.; Hua, D. H. Design, synthesis, and bioevaluation of viral 3C and 3C-like protease inhibitors. *Bioorg. Med. Chem. Lett.* **2013**, *23*, 6317–6320. (l) Mandadapu, S. R.; Weerawarna, P. M.; Prior, A. M.; Uy, R. A. Z.; Aravapalli, S.; Alliston, K. R.; Lushington, G. H.; Kim, Y. j.; Hua, D. H.; Chang, K. O.; Groutas, W. C. Macrocyclic inhibitors of 3C and 3C-like proteases of picornavirus, norovirus, and coronavirus. *Bioorg. Med. Chem. Lett.* **2013**, *23*, 3709–3712.

(6) (a) Dragovich, P. S.; Prins, T. J.; Zhou, R.; Brown, E. L.; Maldonado, F. C.; Fuhrman, S. A.; Zalman, L. S.; Tuntland, T.; Lee, C. A.; Patick, A. K.; Matthews, D. A.; Hendrickson, T. F.; Kosa, M. B.; Liu, B.; Batugo, M. R.; Gleeson, J. R.; Sakata, S. K.; Chen, L. J.; Guzman, M. C.; Meador, J. W.; Ferre, R. A.; Worland, S. T. Structure-based design, synthesis, and biological evaluation of irreversible human rhinovirus 3C protease inhibitors. 6. Structure-activity studies of orally bioavailable, 2-Pyridone-containing peptidomimetics. *J. Med. Chem.* **2002**, *45*, 1607–1623. (b) Zhang, X.; Song, Z.; Qin, B.; Zhang, X.; Chen, L.; Hu, Y.; Yuan, Z. Rupintrivir is a promising candidate for treating severe cases of enterovirus-71 infection: Evaluation of antiviral efficacy in a murine infection model. *Antiviral Res.* **2013**, *97*, 264–269. (c) Patick, A. K.; Binford, S. L.; Brothers, M. A.; Jackson, R. L.; Ford, C. E.; Diem, M. D.; Maldonado, F.; Dragovich, P. S.; Zhou, R.; Prins, T. J.; Fuhrman, S. A.; Meador, J. W.; Zalman, L. S.; Matthews, D. A.; Worland, S. T. In vitro antiviral activity of AG7088, a potent inhibitor of human rhinovirus 3C protease. *Antimicrob. Agents Chemother.* **1999**, *43*, 2444–2450. (d) Wang, J.; Fan, T.; Yao, X.; Wu, Z.; Guo, L.; Lei, L.; Wang, J.; Wang, M.; Jin, Q.; Cui, S. Crystal structures of enterovirus 71 3C protease complexed with rupintrivir reveal the roles of catalytically important residues. *J. Virology.* **2011**, *85*, 10021–10030. (e) Lu, G.; Qi, J.; Chen, Z.; Xu, X.; Gao, F.; Lin, D.; Qian, W.; Liu, H.; Jiang, H.; Yan, J.; Gao, G. F. Enterovirus 71 and Coxsackievirus A16 3C proteases: binding to Rupintrivir and their substrates and anti-hand, foot, and mouth disease virus drug design. *J. Virology.* **2011**, *85*, 10319–10331. (f) Wu, C.; Cai, Q.; Chen, C.; Li, N.; Peng, X.; Cai, Y.; Yin, K.; Chen, X.; Wang, X.; Zhang, R.; Liu, L.; Chen, S.; Li, J.; Lin, T. Structures of Enterovirus 71 3C proteinase (strain E2004104-TW-CDC) and its complex with rupintrivir. *Acta Crystallogr., Sect. D: Biol. Crystallogr.* **2013**, *69*, 866–871. (g) Cui, S.; Wang, J.; Fan, T.; Qin, B.; Guo, L.; Lei, X.; Wang, J.; Wang, M.; Jin, Q. Crystal structure of human enterovirus 71 3C protease. *J. Mol. Biol.* **2011**, *408*, 449–461.

(7) (a) Zhang, K. E.; Hee, B.; Lee, C. A.; Liang, B.; Potts, B. C. M. Liquid Chromatography-Mass spectrometry and liquid Chromatography-NMR characterization of in vitro metabolites of a potent and irreversible peptidomimetic inhibitor of rhinovirus 3C protease. *Drug Metab. Dispos.* **2001**, *29*, 729–734. (b) Dragovich, P. S.; Prins, T. J.; Zhou, R.; Webber, S. E.; Marakovits, J. T.; Fuhrman, S. A.; Patick, A. K.; Matthews, D. A.; Lee, C. A.; Ford, C. E.; Burke, B. J.; Rejto, P. A.; Hendrickson, T. F.; Tuntland, T.; Brown, E. L.; Meador, J. W., III; Ferre, R. A.; Harr, J. E.; Kosa, M. B.; Worland, S. T. Structure-based design, synthesis, and biological evaluation of irreversible human rhinovirus 3C protease inhibitors. 4. Incorporation of P1 lactam moieties as L-glutamine replacements. *J. Med. Chem.* **1999**, *42*, 1213–1224. (c) Hsyu, P. H.; Pithavala, Y. K.; Gersten, M.; Penning, C. A.; Kerr, B. M. Pharmacokinetics and safety of an antirhinoviral agent, Rupintrivir, in healthy volunteers. *Antimicrob. Agents Chemother.* **2002**, *46*, 392–397. (d) Shie, J. J.; Fang, J. M.; Kuo, T. H.; Kuo, C. J.; Liang, P. H.; Huang, H. J.; Wu, Y. T.; Jan, J. T.; Cheng, Y. S. E.; Wong, C. H. Inhibition of the severe acute respiratory syndrome 3CL protease by peptidomimetic α , β -unsaturated esters. *Bioorg. Med. Chem.* **2005**, *13*, 5240–5252.

(8) (a) Zhou, P.; Yang, X. L.; Wang, X. G.; Hu, B.; Zhang, L.; Zhang, W.; Si, H. R.; Zhu, Y.; Li, B.; Huang, C. L.; Chen, H. D.; Chen, J.; Luo, Y.; Guo, H.; Jiang, R. D.; Liu, M. Q.; Chen, Y.; Shen, X. R.; Wang, X.; Zheng, X. S.; Zhao, K.; Chen, Q. J.; Deng, F.; Liu, L. L.; Yan, B.; Zhan, F.

- X.; Wang, Y. Y.; Xiao, G. F.; Shi, Z. L. A pneumonia outbreak associated with a new coronavirus of probable bat origin. *Nature* **2020**, *579*, 270–273. (b) Wu, F.; Zhao, S.; Yu, B.; Chen, Y. M.; Wang, W.; Song, Z. G.; Hu, Y.; Tao, Z. W.; Tian, J. H.; Pei, Y. Y.; Yuan, M. L.; Zhang, Y. L.; Dai, F. H.; Liu, Y.; Wang, Q. M.; Zheng, J. J.; Xu, L.; Holmes, E. C.; Zhang, Y. Z. A new coronavirus associated with human respiratory disease in China. *Nature* **2020**, *579*, 265–269. (c) Chinazzi, M.; Davis, J. T.; Ajelli, M.; Gioannini, C.; Litvinova, M.; Merler, S.; Pastore y Piontti, A.; Mu, K.; Rossi, L.; Sun, K.; Viboud, C.; Xiong, X.; Yu, H.; Halloran, M. E.; Longini, I. M.; Vespignani, A. The effect of travel restrictions on the spread of the 2019 novel coronavirus (COVID-19) outbreak. *Science* **2020**, *368*, 395–400. (d) Ledford, H. Coronavirus breakthrough: dexamethasone is first drug shown to save lives. *Nature* **2020**, *582*, 469. (e) Kupferschmidt, K. Global trial eliminates drugs, pivots to new ones. *Science* **2020**, *370*, 388–389.
- (9) (a) Ghosh, A. K.; Brindisi, M.; Shahabi, D.; Chapman, M. E.; Mesecar, A. D. Drug development and medicinal chemistry efforts toward SARS-coronavirus and Covid-19 therapeutics. *ChemMedChem* **2020**, *15*, 907–932. (b) Zhang, L.; Lin, D.; Sun, X.; Curth, U.; Drosten, C.; Sauerhering, L.; Becker, S.; Rox, K.; Hilgenfeld, R. Crystal structure of SARS-CoV-2 main protease provides a basis for design of improved alpha-ketoamide inhibitors. *Science* **2020**, *368*, 409–412. (c) Jin, Z.; Du, X.; Xu, Y.; Deng, Y.; Liu, M.; Zhao, Y.; Zhang, B.; Li, X.; Zhang, L.; Peng, C.; Duan, Y.; Yu, J.; Wang, L.; Yang, K.; Liu, F.; Jiang, R.; Yang, X.; You, T.; Liu, X.; Yang, X.; Bai, F.; Liu, H.; Liu, X.; Guddat, L. W.; Xu, W.; Xiao, G.; Qin, C.; Shi, Z.; Jiang, H.; Rao, Z.; Yang, H. Structure of M(pro) from SARS-CoV-2 and discovery of its inhibitors. *Nature* **2020**, *582*, 289–293. (d) Dai, W.; Zhang, B.; Jiang, X. M.; Su, H.; Li, J.; Zhao, Y.; Xie, X.; Jin, Z.; Peng, J.; Liu, F.; Li, C.; Li, Y.; Bai, F.; Wang, H.; Cheng, X.; Cen, X.; Hu, S.; Yang, X.; Wang, J.; Liu, X.; Xiao, G.; Jiang, H.; Rao, Z.; Zhang, L. K.; Xu, Y.; Yang, H.; Liu, H. Structure-based design of antiviral drug candidates targeting the SARS-CoV-2 main protease. *Science* **2020**, *368*, 1331–1335.
- (10) (a) Yuan, J.; Shen, L.; Wu, J.; Zou, X.; Gu, J.; Chen, J.; Mao, L. Enterovirus A71 proteins: structure and function. *Front. Microbiol.* **2018**, *9*, 286. (b) Tyagi, A.; Nigam, S.; Chauhan, R. S. A concise review of baseline facts of SARS-CoV-2 for interdisciplinary research. *ChemistrySelect* **2020**, *5*, 10897–10923. (c) Anand, K.; Palm, G. J.; Mesters, J. R.; Siddell, S. G.; Ziebuhr, J.; Hilgenfeld, R. Structure of coronavirus main proteinase reveals combination of a chymotrypsin fold with an extra α -helical domain. *EMBO J.* **2002**, *21*, 3213–3224.
- (11) (a) Yang, K. S.; Ma, X. R.; Ma, Y.; Alugubelli, Y. R.; Scott, D. A.; Vatanserver, E. C.; Drelich, A. K.; Sankaran, B.; Geng, Z. Z.; Blankenship, L. R.; Ward, H. E.; Sheng, Y. J.; Hsu, J. C.; Kratch, K. C.; Zhao, B.; Hayatshahi, H. S.; Liu, J.; Li, P.; Fierke, C. A.; Tseng, C. K.; Xu, S.; Liu, W. R. A quick route to multiple highly potent SARS-CoV-2 main protease inhibitors. *ChemMedChem* **2021**, *15*, 1–8. (b) Hoffman, R. L.; Kania, R. S.; Brothers, M. A.; Davies, J. F.; Ferre, R. A.; Gajiwala, K. S.; He, M.; Hogan, R. J.; Kozminski, K.; Li, L. Y.; Lockner, J. W.; Lou, J.; Marra, M. T.; Mitchell, L. J., Jr; Murray, B. W.; Nieman, J. A.; Noell, S.; Planken, S. P.; Rowe, T.; Ryan, K.; Smith, G. J., III; Solowiej, J. E.; Steppan, C. M.; Taggart, B. Discovery of Ketone-Based Covalent Inhibitors of Coronavirus 3CL Proteases for the Potential Therapeutic Treatment of COVID-19. *J. Med. Chem.* **2020**, *63*, 12725–12747. (c) Vuong, W.; Khan, M. B.; Fischer, C.; Arutyunova, E.; Lamer, T.; Shields, J.; Saffran, H. A.; McKay, R. T.; van Belkum, M. J.; Joyce, M. A.; Young, H. S.; Tyrrell, D. L.; Vederas, J. C.; Lemieux, M. J. Feline coronavirus drug inhibits the main protease of SARS-CoV-2 and blocks virus replication. *Nat. Commun.* **2020**, *11*, 4282.
- (12) (a) Ward, K. W.; Azzarano, L. M.; Evans, C. A.; Smith, B. R. Apparent absolute oral bioavailability in excess of 100% for a vitronectin receptor antagonist (SB-265123) in rat. I. Investigation of potential experimental and mechanistic explanations. *Xenobiotica* **2004**, *34*, 353–366. (b) Ward, K. W.; Hardy, L. B.; Kehler, J. R.; Azzarano, L. M.; Smith, B. R. Apparent absolute oral bioavailability in excess of 100% for a vitronectin receptor antagonist (SB-265123) in rat. II. Studies implicating transporter-mediated intestinal secretion. *Xenobiotica* **2004**, *34*, 367–377.
- (13) Wang, Q. S.; Zhang, K. H.; Cui, Y.; Wang, Z. J.; Pan, Q. Y.; Liu, K.; Sun, B.; Zhou, H.; Li, M. J.; Xu, Q.; Xu, C. Y.; Yu, F.; He, J. H. Upgrade of macromolecular crystallography beamline BL17U1 at SSRF. *Nucl. Sci. Tech.* **2018**, *29*, 681–687.
- (14) Minor, W.; Cymborowski, M.; Otwinowski, Z.; Chruszcz, M. HKL-3000: the integration of data reduction and structure solution from diffraction images to an initial model in minutes. *Acta Crystallogr., Sect. D: Biol. Crystallogr.* **2006**, *62*, 859–866.
- (15) McCoy, A. J.; Grosse-Kunstleve, R. W.; Adams, P. D.; Winn, M. D.; Storoni, L. C.; Read, R. J. Phaser crystallographic software. *J. Appl. Crystallogr.* **2007**, *40*, 658–674.
- (16) Emsley, P.; Cowtan, K. Coot: model-building tools for molecular graphics. *Acta Crystallogr., Sect. D: Biol. Crystallogr.* **2004**, *60*, 2126–2132.
- (17) Adams, P. D.; Grosse-Kunstleve, R. W.; Hung, L. W.; Ioerger, T. R.; McCoy, A. J.; Moriarty, N. W.; Read, R. J.; Sacchettini, J. C.; Sauter, N. K.; Terwilliger, T. C. PHENIX: building new software for automated crystallographic structure determination. *Acta Crystallogr., Sect. D: Biol. Crystallogr.* **2002**, *58*, 1948–1954.
- (18) Su, H. X.; Yao, S.; Zhao, W. F.; Li, M. J.; Liu, J.; Shang, W. J.; Xie, H.; Ke, C. Q.; Hu, H. C.; Gao, M. N.; Yu, K. Q.; Liu, H.; Shen, J. S.; Tang, W.; Zhang, L. K.; Xiao, G. F.; Ni, L.; Wang, D. W.; Zuo, J. P.; Jiang, H. L.; Bai, F.; Wu, Y.; Ye, Y.; Xu, Y. C. Anti-SARS-CoV-2 activities in vitro of Shuanghuanglian preparations and bioactive ingredients. *Acta Pharmacol. Sin.* **2020**, *41*, 1167–1177.
- (19) Wang, M.; Cao, R.; Zhang, L.; Yang, X.; Liu, J.; Xu, M.; Shi, Z.; Hu, Z.; Zhong, W.; Xiao, G. Remdesivir and chloroquine effectively inhibit the recently emerged novel coronavirus (2019-nCoV) in vitro. *Cell Res.* **2020**, *30*, 269–271.
- (20) (a) Sun, L.; Meijer, A.; Froeyen, M.; Zhang, L.; Thibaut, H. J.; Baggen, J.; George, S.; Vernachio, J.; van Kuppeveld, F. J. M.; Leyssen, P.; Hilgenfeld, R.; Neyts, J.; Delang, L. Antiviral activity of broad-spectrum and enterovirus-specific inhibitors against clinical isolates of enterovirus D68. *Antimicrob. Agents Chemother.* **2015**, *59*, 7782–7785. (b) Aguado, L.; Thibaut, H. J.; Priego, E.-M.; Jimeno, M.-L.; Camarasa, M.-J.; Neyts, J.; Pérez-Pérez, M.-J. 9-Arylpurines as a novel class of enterovirus inhibitors. *J. Med. Chem.* **2010**, *53*, 316–324. (c) Costa, L. D.; Scheers, E.; Coluccia, A.; Casulli, A.; Roche, M.; Giorgio, C. D.; Neyts, J.; Terme, T.; Cirilli, R.; Regina, G. L.; Silvestri, R.; Mirabelli, C.; Vanelle, P. Structure-Based Drug Design of Potent Pyrazole Derivatives against Rhinovirus Replication. *J. Med. Chem.* **2018**, *61*, 8402–8416.